

# California Oil Spill Study and Evaluation Program (COSSEP) RFP #P1975001

## Improving Oil Detection Capability Using a Portable, UAS-based SCAT Reconnaissance System



Final Report to California Department of Fish and Wildlife COSSEP

Reporting Period: July 1, 2019 – November 15, 2021

Mark Hess  
Director of Operations, Ocean Imaging

James White  
RS/GIS Analyst, Ocean Imaging

Judd Muskat  
CDFW-OSPR Senior Environmental Scientist (Specialist)

*Ocean Imaging*

13976 West Bowles Avenue, Suite 100, Littleton CO 80127 Phone: 303-948-5272 Fax: 303-948-2549  
www.oceani.com

# Table of Contents

Executive Summary.....	2
1.0 Introduction .....	2
2.0 sUAS Hardware and Software Procurement and Development.....	3
3.0 Data Collection and Methods .....	7
3.1 Stage 1: Preliminary Test Flights and Field Work .....	7
3.2 Stage 2: sUAS Flights and Field Work .....	7
3.3 Study Site 1: McKittrick Tar Pits.....	8
3.4 Study Site 2: Carpinteria Beach .....	12
3.5 Multispectral Data Processing and Image Mosaicking .....	17
3.6 Thermal Infrared Data Processing and Image Mosaicking .....	18
3.7 Ultraviolet Data Processing and Image Mosaicking .....	18
3.8 Oil Detection Algorithm Development .....	19
3.9 Multispectral Oil Extraction Equation.....	22
3.10 SAVI Mask .....	24
3.11 TIR Mask.....	24
4.0 Results.....	26
4.1 Oil Identification Using UV.....	26
4.2 Oil Identification Using MS and TIR .....	27
5.0 Discussion .....	32
5.1 Further Research and Algorithm Refinement.....	32
5.2 Proposed Operational System .....	33
Appendix A: Equipment Inventory.....	35
Appendix B Imagery and Probability Oil Maps .....	36

# Executive Summary

Shoreline Cleanup Assessment Technique (SCAT) operations are a fundamental part of oil spill response for both marine and inland spills. Presently, there is an effort within the California Department of Fish and Wildlife (CDFW) Oil Spill Prevention and Response (OSPR) division to advance the current state of small Unmanned Aircraft System (sUAS) reconnaissance for SCAT operations. The project aimed to incorporate more sophisticated sensors into a portable sUAS to assess the efficacy of the enhanced equipment and novel oil detection algorithms designed to help responders and SCAT teams more quickly and accurately identify and assess oiled areas in shoreline and inland waterway habitats. The system was built using CDFW's existing sUAS platform and multispectral camera adding two additional cameras imaging in the ultraviolet and thermal infrared wavelengths. Custom software was written to facilitate the incorporation of these sensors and processing of the resulting data. Ultimately two study locations in California (the McKittrick natural oil seeps and a natural seep oiled beach below Carpinteria Bluffs) were chosen that offered fresh and weathered oil targets needed for the development of an oil detection and classification algorithm. The ultraviolet wavelengths did not prove to be as useful as the visible, near infrared and thermal infrared bands in the detection and isolation of oil-covered substrate and vegetation. A multistep image processing algorithm was developed using these sensor bands that effectively classified high probability oil targets with minimal false positive identifications. The results of the study showed that a sUAS equipped with a 5-channel multispectral and thermal infrared imaging system could provide accurate and easy to interpret oil identification information to SCAT and other response workers at a reasonable cost.

## 1.0 Introduction

Efficiency in oil spill Shoreline Cleanup Assessment Technique (SCAT) and Natural Resource Damage Assessment (NRDA) operations is becoming increasingly more important for oil spill response. Prior to this project California Department of Fish and Wildlife (CDFW) Office of Spill Prevention and Response (OSPR), was working to advance the current state of small Unmanned Aircraft System sUAS reconnaissance for SCAT operations. This project aimed to study the incorporation of more sophisticated sensors into a portable sUAS, so that oil spill responders and SCAT teams can more quickly and accurately identify and assess oiled areas in shoreline and inland waterway habitats, including areas with limited or no access due to health and safety restrictions (e.g., small pocket beaches, steep riverbanks and rocky intertidal areas). The research was designed around and expanded upon the results of OSPR's initial efforts by 1) Utilizing the existing OSPR equipment for further study and development; 2) enhancing the imaging system's accuracy of separating true oiled areas from false targets through the addition of a specially configured ultraviolet-sensing camera and a thermal infrared camera; 3) conduct additional experiments for algorithm development in locations with actual, naturally formed oiled shoreline targets originating from oil seeps in California. The core research was centered around how the integration of an ultraviolet (UV) be fitted with specialized UV-band pass filters and a thermal infrared (TIR) camera into a sUAS would improve oil detection and mapping capability over the single-camera system OSPR presently had. A future oil mapping sUAS resulting from this study would offer CDFW-OSPR unprecedented capability to remotely locate and map oiled-areas in support of SCAT and NRDA.

The system configured and developed for this research utilized OSPR's existing sUAS platform (*DJI Matrice 100*: <https://www.dji.com/matrice100>) originally equipped with a MicaSense RedEdge-M multispectral camera (MS). The limited budget did not allow for the purchase of a different, more sophisticated sUAS platform. The project expanded the sensor package to include the Zenmuse XT 30HZ V2 and JAI CM-140GE UV cameras. At the time of project starting, the Zenmuse XT was the only available TIR camera compatible with the M100 platform. The JAI CM-140GE UV camera was selected for its affordability and because an Application Programming Interface (API) package was available for the camera that allowed for customization to the camera shutter triggering mechanism. Although the available budget and existing CDFW DJI Matrice 100 (M100) platform limited the ability to fully and permanently integrate all three sensors onto the sUAS, steps to build an operational multi-sensor system can be taken in the future with later model sUAS.

This report is the final documentation of the project as outlined in the State of California Standard Agreement number P1975001. The project dates stated in the original contract were delayed due to California Department of Fish and Wildlife-Office of Oil Spill Prevention and Response (CDFW-OSPR) administrative delays. The original contract scheduled to begin in January of 2019 was moved to July 1, 2019. Work on the first phase of the project began in the early fall of 2019. Phase one was extended further by several months due to travel and staffing restraints created by the COVID-19 pandemic. The first phase of the project is discussed in the progress report - included as Attachment A- submitted on December 1, 2020, covering the working dates between September 28, 2019, through December 1, 2020. Also due to pandemic-related restrictions, the period end of this contract was extended to June 30, 2022. This final documentation includes the project results, discussion and recommendations for future study and system development.

## 2.0 sUAS Hardware and Software Procurement and Development

All necessary Single Board Computer (SBC), camera, flight control and mounting equipment were first shipped to the hardware-software engineer and, to the extent that was possible, integrated into the DJI Matrice 100 (M100) system. This included the Zenmuse XT 30HZ V2 TIR camera with a 13mm lens, the JAI CM-140GE UV Camera with the UKA Optics C-Mount, 6mm UV-compatible Lens (JAI-UV) as well as the MicaSense RedEdge-M MS camera system. UV bandpass filters in the 324 nm, 365 nm and 405 nm ranges were purchased and tested on the UV camera. Additional hardware was acquired to build the power/control/communication harness for the UV camera. A calibration panel for the RedEdge MS camera was also purchased, for one was not included with the M100/MicaSense package provided by OSPR. The M100 came with four batteries, however one of the four reported errors when connected to the DJI system and therefore was not used for any of the flights. A complete equipment list is in Appendix A.

The initial configuration and development of the sensor system mounted on the M100 is discussed in detail in Attachment A. The original concept was to integrate the SBC output of the JAI-UV live radiometric video data with the N1 video encoder, which is part of the M100 system. However, it was discovered that the N1 controller/encoder in conjunction with the M100 only allows for communication with and data streaming from a single camera system. On this platform the TIR camera was the only device integrated with the M100 and N1. Further investigation revealed that on the M100/N1 platform, the MicaSense MS system cannot acquire in synchronization with other cameras systems. In addition to these limitations, several other functions are not possible using the M100/N1 platform. The following list includes the most notable of these missing functionalities:

- Ability to trigger all camera systems through a single mechanism
- Ability to record GPS/IMU data for all camera data frames from a single GPS/IMU source
- Ability to stream UV or MS image data down to DJI/M100 controller for real-time viewing on operator's controller device
- Capability for operator to toggle between MS, TIR and UV image/data stream
- Show real-time location/GPS information of DJI UAS in the data stream and mark on image snapshots/screen grabs
- Ability to co-register image data in real time to facilitate faster image processing and oil identification

Due to these M100/N1 shortcomings, custom camera triggering, and image acquisition software development was required in order to have all three camera systems acquire data simultaneously. After the thorough review process, an Ubuntu, 64-bit Linux-based Raspberry Pi (RPI) SBC was selected and mounted on the UAS platform to drive the acquisition and storage of the imagery acquired by the MS and JAI-UV cameras. The TIR camera was controlled by the DJI N1 controller and associated software. A power/communication harness was then designed and built along with software to enable the UV camera to do the following:

- Communicate with the SBC
- Draw power from the M100 system

- Write captured image frames/files to SD Card or storage device on SBC
- Be triggered to acquire data at same time as MS and TIR cameras
- Capture GPS/INS data from MS camera system and match the data header format acquired and stored with format of the MS camera.

To accommodate for the limitations of the N1 interface, the JAI-UV was designed along with the software in the SBC to use the MS camera as the shutter triggering control device as well as ingest the GPS/IMU data from the MS and write to the JAI-UV header files associated with each JAI-UV data frame file. The TIR camera operates independently from the other two cameras, but it was set to trigger the shutter (acquire image data) at one second intervals or faster. Software was written to extract the time coincident TIR image frames that best match the frames acquired by the other two cameras. For the purposes of this project, it was decided that all data would be downloaded post-flight from the different cameras from either the SD cards or via Wi-Fi interface from the SBC and/or MicaSense devices. Table 1 outlines the resulting camera interface specifications based on the capabilities of the M100 and N1 video encoder. Table 2 lists the wavelengths and bandwidths of each of the sensors on the camera systems.

Table 1. Camera interface specifications

Camera	Power Source	Data Capture and Video Streaming	Storage and File Format	Acquisition Triggering	GPS/IMU Source
TIR - Zenmuse XT640x512, 30Hz	DJI XS Series Gimbal	DJI N1 / DJI remote control	Micro SD card (up to 32 Gb) / GeoTIFF	Configured by DJI Go App or equivalent	DJI GPS antenna / DJI flight controller
Multispectral – MicaSense RedEdge 1280x960, 1Hz	power adapter module, which is powered via extra XT30 power feed	Wi-Fi access point only	SDHC (32 Gb) /12-bit DNG or 16-bit GeoTIFF	Configured by MicaSense web application or Atlas application on camera via Wi-Fi	MicaSense GPS antenna / MicaSense IMU
UV - JAI CM-140GE-UV1392x1040, 16Hz	custom RPI 'hat', which is powered via extra XT30 power feed	Wi-Fi access point only	Micro SD card (32 Gb) / 10-bit BIL	Synchronized to trigger on every RedEdge camera trigger	Retrieved from MicaSense GPS/IMU through Ethernet interface

Table 2. Camera sensor specifications

Camera	Band Name	Band Number*	Center Wavelength (nm)	Bandwidth (nm)
MicaSense RedEdge-M	Red	1	668	14
MicaSense RedEdge-M	Green	2	560	27
MicaSense RedEdge-M	Blue	3	475	32
MicaSense RedEdge-M	Red Edge	4	717	12
MicaSense RedEdge-M	Near IR	5	842	57
Zenmuse XT	TIR	1	10500	6000
JAI CM-140GE	UV	1	324, 365, 405	75, 65, 15

\* The band order shown in the table reflects the order created in the MicaSense image mosaics used in the data processing and algorithm development.

The M100 also has a limited payload/weight capability which was just barely enough to carry the camera payload designed for this project. Recommendations on a more suitable UAS platform for operational use will be presented in more detail in the Discussion section. For the purposes of this research, however, the M100 with the described use modifications here was found to be suitable to assess the enhanced camera systems flown on a sUAS as an oil detection tool. Additional modifications were made following the first stage of the project to redesign some of the camera mounts and power cables to lighten the payload and improve the weight distribution of the cameras and SBC on the M100 platform. The intent was to achieve maximum flight time of the system given the payload limitations of the M100 platform.

Since the MS camera came pre-mounted from OSPR at a specific viewing angle and served as the ‘primary’ camera in terms of acquisition triggering and geolocating the data, the JAI-UV Field of View (FOV) and viewing angle were aligned to best match that of the MS. This allowed for the JAI-UV-generated data frames to geospatially correspond to that of the MicaSense so the two data sets could be co-georeferenced as easily as possible. This was necessary to create and test UV-MS band combinations that might help isolate the oil from non-oiled vegetation and substrates in the image mosaics. The cameras were ‘boresighted’ to each other by

mounting the sUAS system to a fixed platform and imaging an optically and thermally reflective grid using all the three sensors. The JAIV-UV camera needed to be mounted at a 12° forward-looking angle to best match the viewing angle and FOV of the MS camera. A custom, lightweight mount was created for the JAI-UV camera to secure the camera to this viewing angle.

The TIR camera viewing angle is controlled by a gimbal that is part of the Zenmuse system. Unfortunately, the DJI/Zenmuse controlling software compatible with the M100 does not allow the operator to set the camera to a fixed, numerical look angle. Therefore, the downward viewing angle of the TIR camera had to be manually estimated and set before each flight. This limitation created challenges when working to align the TIR data with the data from the other two camera systems and is a clear deficiency in the TIR gimble/camera controller application. Figure 1 shows the final configuration of the devices mounted on the M100 with the custom UV camera mount.



Figure 1. M100 with camera systems and SBC installed (A=JAI CM-140GE-UV, B=RPI SBC, C=MicaSense RedEdge MS, D= Zenmuse XT TIR). Bottom left image shows custom mount for UV camera (B). Bottom right image shows final camera alignment and SBC placement.

Final software development included the writing of Python and C++ code to aid in the mosaicking, co-registering and batch classification of the data from the three cameras. PIX4Dmapper software (version 4.6.4 - <https://www.pix4d.com/product/pix4dmapper-photogrammetry-software>) and custom Python scripts were used to align the bands and mosaic the individual MS and TIR data frames. A Windows-based application was developed to convert the UV image data from its native format (.bip) to geospatially corrected GeoTIFF file with a WGS1984 coordinate system. Python and Esri's ArcGIS Pro were predominantly used for the final image processing, algorithm development and oil classification work.

The mission planning and flight control was driven by the MicaSense Atlas application; however, more capable flight planning and control applications were investigated in order to improve mission planning as well as better facilitate the manual control of the DJI platform and data acquisition. Suggestions on the most appropriate and effective tools for an operational system follows in the Discussion section.

## **3.0 Data Collection and Methods**

### **3.1 Stage 1: Preliminary Test Flights and Field Work**

Details on the first stage of test flights and subsequent system development work are outlined in the Phase 1 progress report - Attachment A. Following the installation and integration of the cameras, initial test flights were performed by Ocean Imaging (OI) in Colorado to assess the base-level performance of the M100 and payload of sensors. Initial flights were performed to ascertain the maximum flight time of the system given the 'heavy', three-camera and SBC payload. Several test flights established that the fully loaded M100 can safely operate for 13-16 minutes on a single battery. Subsequent flights were executed to test the boresighting and simultaneous data acquisition of the three cameras. Achieving perfect optical alignment and image frame overlap of all three camera systems was not possible due to the different image frame and CCD pixel sizes, however, the acquisition of image frames with sufficient geospatial agreement was achieved to facilitate three-camera band co-registration without too much post processing. Sample, preliminary imagery acquired over a non-oiled target is shown in Attachment A. As part of the stage 1, OI continued to perform additional test flights to gather sample image data for both data processing workflow design and to determine the best flight planning, control and post processing solutions. This process took roughly two to three months longer than expected due to weather and other restraints created by Colorado COVID-19 mandates.

### **3.2 Stage 2: sUAS Flights and Field Work**

Due to restrictions in place because of the COVID-19 pandemic, the stage 2 and 3 three flight locations were changed from the original experimental plan and combined into a single trip over one week's time. The first location selected was located near the McKittrick Tar Pits 31 miles west of Bakersfield, California. This site is on the Chevron North America Exploration and Production Company property and was accessed and imaged with the permission of Chevron's Land Representative for Cymric and McKittrick. The second site was on the beach in the mid-intertidal zone south of the Carpinteria Bluffs Nature Preserve. Access and permission to fly the sUAS over this site was granted by Santa Barbara County Parks. Both specific study sites were selected due to known, relatively fresh oil in the general areas of interest. In the case of Carpinteria, oil was observed on the beach by CDFW staff a few days before the time of the planned sUAS flights.

### 3.3 Study Site 1: McKittrick Tar Pits

The McKittrick site (Figure 2) was chosen because of the easy access to fresh oil both seeping from the ground and in one spot bubbling up from an opening in the side of a small hill and flowing down into the brush for approximately 30 meters. Many other smaller areas of oil seepage existed in the Area of Study (AOS) including locations to the east of the main seep, to the north in the low scrub area and on the road to the south of the main seep. The surface seeps emanate from the underlying Miocene Monterey Formation. The oil in this region, commonly referred to as 'Monterey Crude' ranges in API gravity from ~12 to 39 - almost asphalt to light crude (California Air Resources Board). The elevation the AOS is roughly 364 meters (~1,195 feet) above sea level. The climate in the region is hot to semi-arid with the predominant vegetation being low scrub, in particular saltbush (*Atriplex lentiformis*).

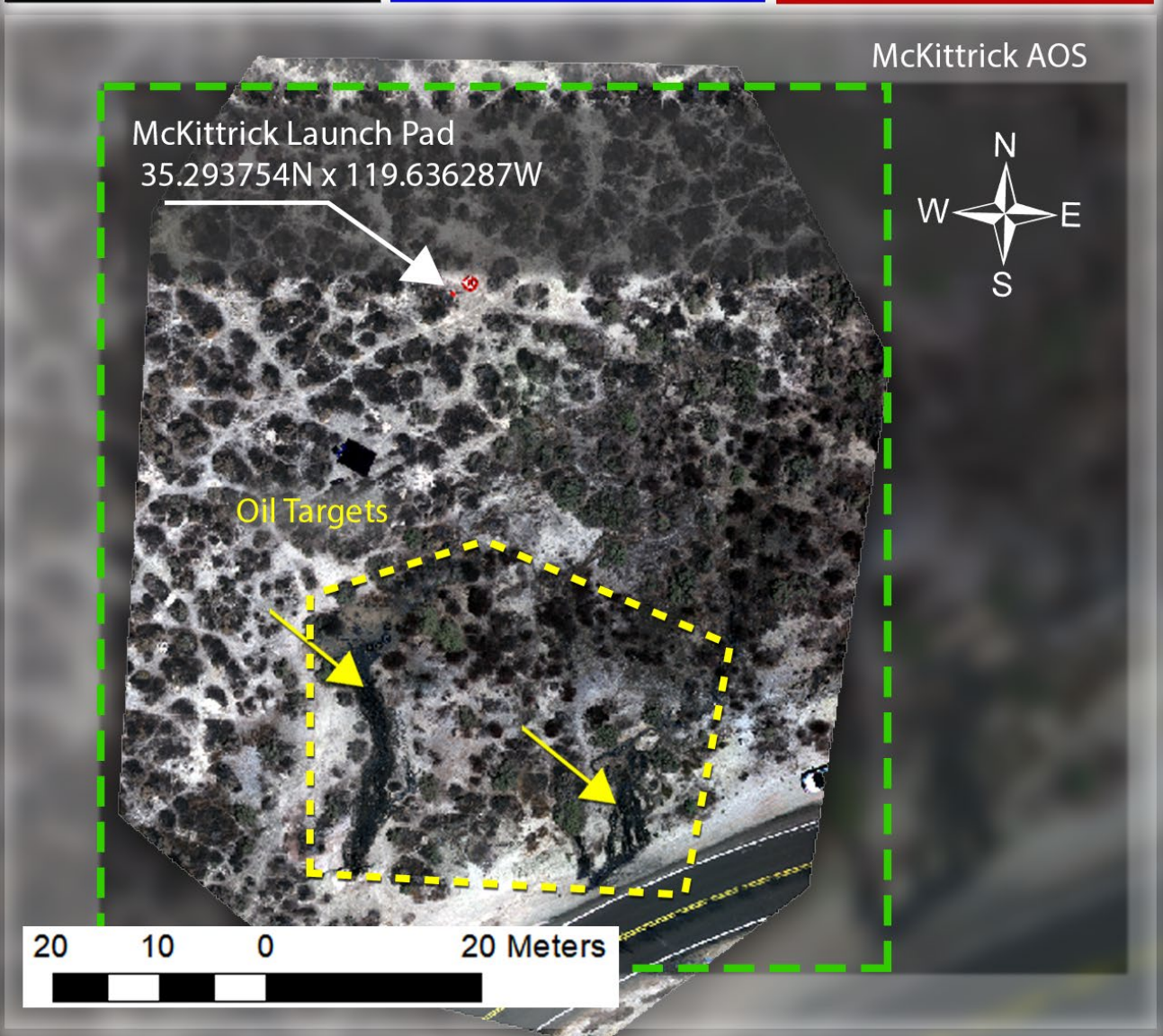
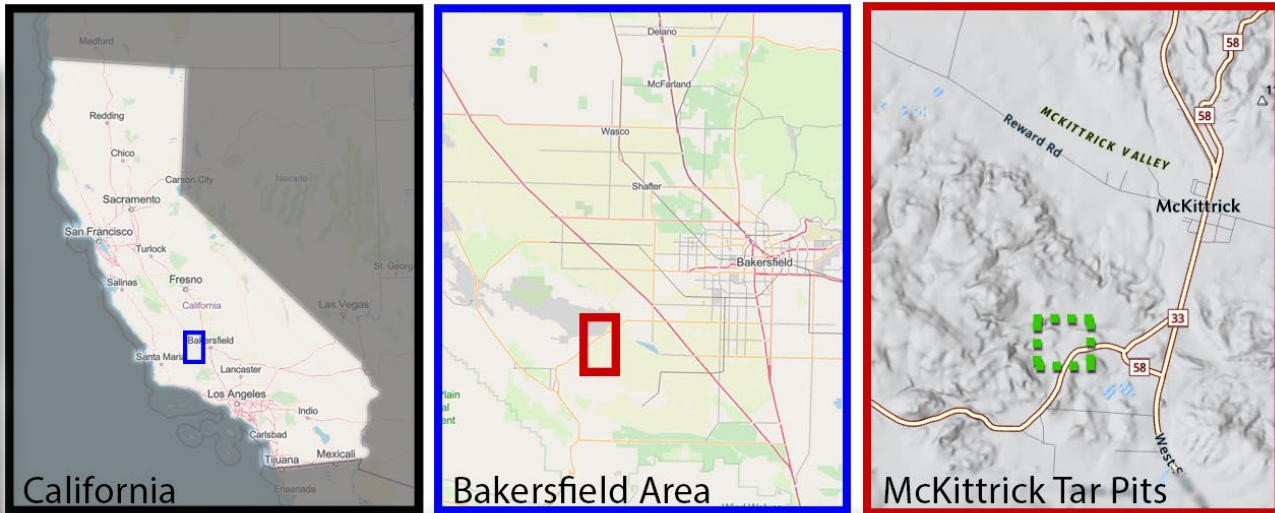


Figure 2. The McKittrick Tar Pits AOS. Green dotted line shows the primary area of the sUAS flights.

The McKittrick flights took place on June 8, 2021, between 11:30 AM PST and 3:00 PM PST. The weather was calm with winds ranging from less than 3 mph to 6 mph with occasional gusts up to 10 mph. The air temperature ranged between 71°F to 83°F and the skies were mostly cloud-free and sunny. Six flight missions were performed

with the M100, three-camera system and one with a smaller, off the shelf *DJI Mavic 2 Enterprise Dual* which carries a payload that includes an integrated HD RGB and TIR camera. A seventh, close range data acquisition session was performed with the M100 instrument held at a height of approximately one meter over a known area of fresh, seeping oil. This was done to provide additional benchmark data as well as to compare the reflectance of the oil as measured by the JAI-UV camera. In the case of McKittrick, the close-range acquisitions were taken over the source of the main seep near the side of the small embankment where the thick, fresh oil was bubbling up from the ground. The Mavic was flown to provide comparative imagery as well as to acquire data of a larger geographical area given its longer flight time capability. Table 3 shows information on each of the data acquisition missions.

Table 3. McKittrick flight information

Flight Number	UV Filter (nm)	Air Speed (m/s)	Altitude (meters)	Pixel Size (cm)*	Frame Overlap	Start Time (PST)	End Time (PST)	Duration (min:sec)	Sky Condition	Wind Speed (mph)
1	365	4.0	40.0	~2.5	75%	11:36 AM	11:41 AM	04:24	sunny, clear	3.5 (5.5 mph gusts)
2	365	4.0	20.0	~1.2	75%	12:21 PM	12:24 PM	03:10	sunny, clear	5.0 (up to 10 mph gusts)
3	365	3.0	10.0	~2.4**	75%	12:47 PM	12:51 PM	03:51	sunny, clear	calm (< 3.0 mph)
4	324	3.0	30.0	~1.8	75%	01:24 PM	01:28 PM	03:40	sunny, clear	calm (< 3.0 mph)
5	324	3.0	20.0	~1.2	75%	01:54 PM	01:57 PM	02:58	sunny, clear	calm (< 3.0 mph)
6	405	3.0	20.0	~1.1	75%	02:20 PM	02:24 PM	04:01	sunny, clear	calm (< 3.0 mph)
Handheld	365	0.0	~1.0	~0.25	N/A	02:44 PM	02:53 PM	09:00	sunny, clear	calm (< 3.0 mph)
Mavic 1	N/A	***	30.48	~1.0	75%	02:55 PM	03:04 PM	09:00	sunny, clear	calm (< 3.0 mph)

\* Size of pixels in the MS image mosaics. The TIR and UV data were subsequently geo-referenced to the MS mosaics and therefore resampled to the same pixel size.

\*\* The PIX4D software used to create the image mosaics from the single image frames automatically re-scaled the data from the 10-meter flight to a coarser cell size than expected.

\*\*\* Mavic air speed not recorded

Prior to each flight, in additions to all the steps and system checks outlined in the Unoccupied Aircraft System Flight Checklist and Log document (DFW 1051), the following preparations were performed:

- New battery installed on the M100, or the existing battery checked to ensure enough charge available for the flight
- Installed desired filter on UV camera lens
- All camera lenses cleaned using commercial-grade lens wipes
- UV camera was manually focused on a target located at the approximate distance corresponding to the altitude of the upcoming flight
- Inserted empty, numbered USB thumb drive in the SBC for data collection
- Altitude, air speed and flight plan configured using the MicaSense Atlas Flight controller application and uploaded to the N1 controller
- Calibrated MicaSense MS camera using MicaSense calibration panel

- Wind speed checked and documented
- TIR camera adjusted and fixed to a nadir-viewing angle

Flight altitudes were chosen to result in imagery with a Ground Sampling Distance (GSD) of 1 cm to 3 cm to best resolve smaller oil features, substrate and vegetation. The AOS was kept to a relatively small area around the seeping oil to preserve battery time and allow as many flights as possible. Each flight was pre-programmed as mapping mission grids into the Atlas flight control software with the pilot at the controls in case of emergency and to perform a controlled landing if necessary. A sample flight grid for the McKittrick site is shown in Figure 3. Following each mission, calibration data were collected again for the MicaSense MS camera system using the calibration panel. The USB drive storing the MS and VU data was then removed, numbered, stored and replaced with a new USB drive to keep all data separate and organized. The TIR data from the DJI SD card was copied to the USB drive corresponding to the same flight. The procedure as outlined above was repeated for each of the seven missions.

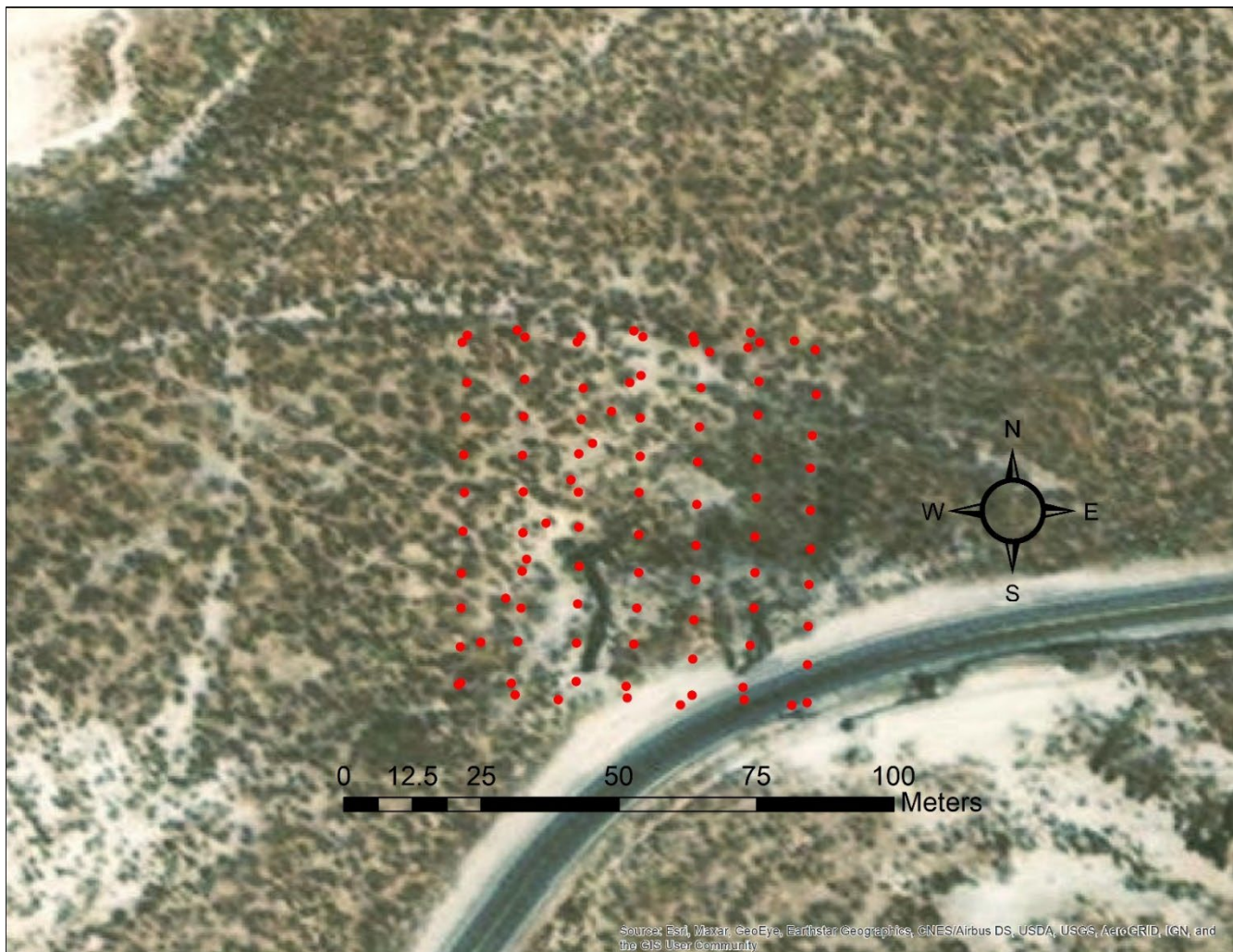


Figure 3. Sample flight path over the McKittrick AOS.

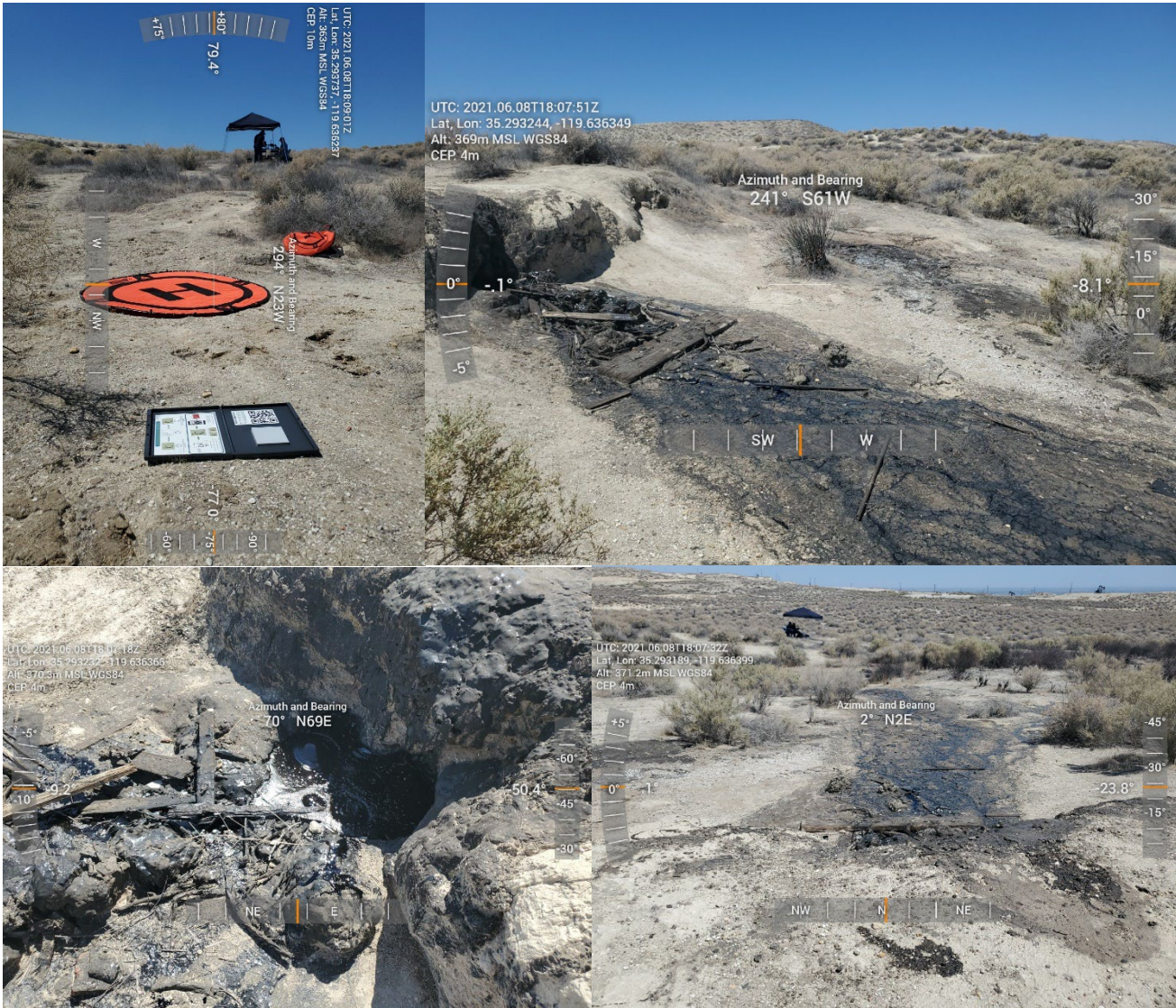
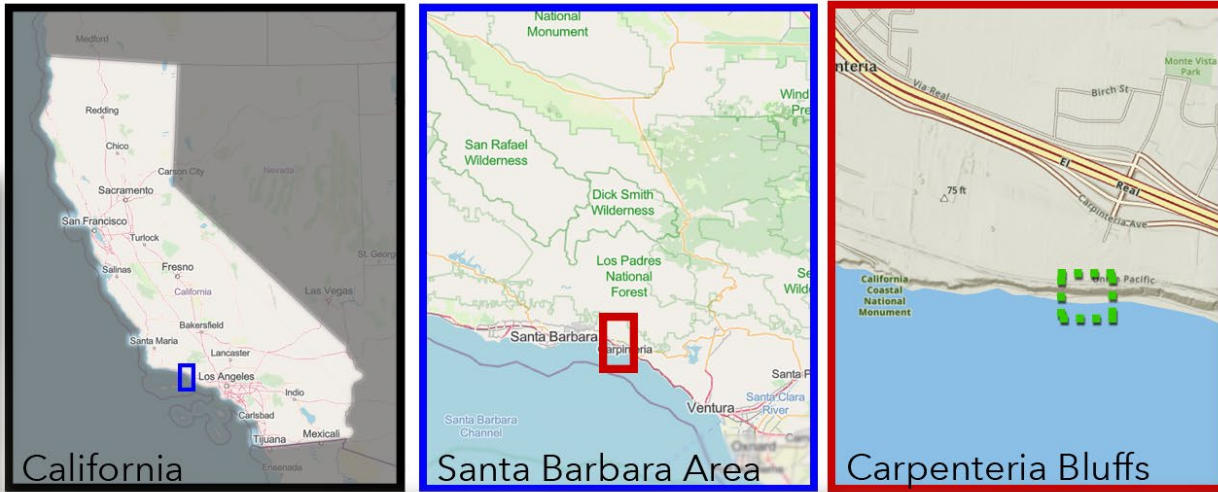


Figure 4. Sample photos of the McKittrick AOS, oil seep area and sUAS launch location.

Photographs and GPS locations of import were taken over the entire AOS for later reference and used for assessment of the image data accuracy as well as algorithm development. Sample photos are shown in Figure 4.

### 3.4 Study Site 2: Carpinteria Beach

A site on the beach below the Carpinteria Bluffs Nature Preserve (Figure 5) was selected as an alternative environment type subject to oiling from offshore or onshore petroleum spills and/or leaks. The Carpinteria region has a warm, arid, Mediterranean-type climate. The substrate in the AOS consisted of sand and rock (both submerged and exposed). The rock was both bare and covered with various flora and fauna such as green algae, barnacles, mussels, sea anemone, limpets, and chitons. Beach wrack was also on the sand consisting primarily of brown algae (kelp) and surfgrass (genus *Phyllospadix*).



Carpenteria Bluffs AOS

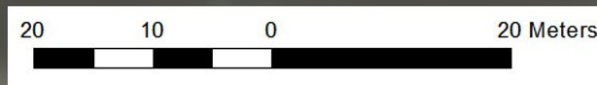


Figure 5. The Carpenteria Bluffs beach AOS. Green dotted line shows the primary area of the sUAS flights.

The oil in this region is the result of the natural oil seeps in the Santa Barbara Channel and surrounding area and is also Monterey Crude from the Monterey Formation. The specific site for the overflights was selected because of the presence of relatively fresh oil and tar balls on the beach above the tide line. Several well-weathered, solid tar balls were found in the upper intertidal zone as were several small (< ~5 cm diameter) globules of relatively fresh oil on the sand or exposed rocks. The primary target of interest was a large mass of fresher oil on the sand right at the tide line. These types of oil masses are commonly called “patties” and will from here forward be referred to as such to distinguish it from the harder, highly weathered tar balls. The size of the patty was approximately 63 cm in diameter and 1.5 cm thick (somewhat large in size for the location). It was found right at the tide mark when arriving at the site and was imaged in the first flight at that location.

To keep using this valuable target without it being submerged by the rising tide, the patty was carefully and safely moved to a location above tide level near an exposed rock and vegetative wrack for the subsequent flights. For flights 3, 4 and 5, additional targets were placed in the area around the larger oil patty. A highly weathered and almost rock-like tar ball was placed next to the fresher oil patty as well as more beach wrack containing a higher percentage of surfgrass. There were also smaller droplets of fresher oil (similar in weathered state to the patty) in the same area as well as a small patch of oil which was partially mixed with sand (Figure 6). The tar ball had a section broken off which exposed less-weathered oil/tar.

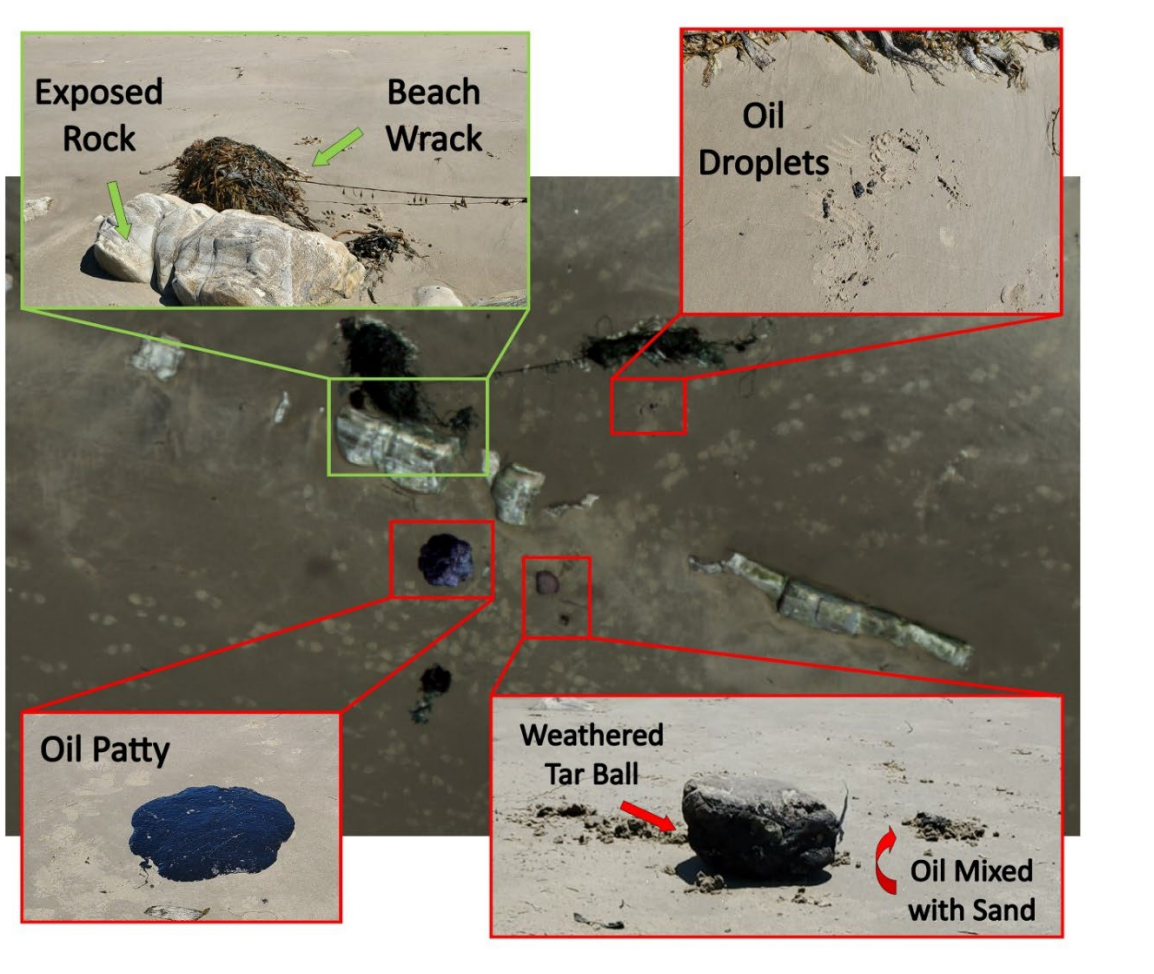


Figure 6. Primary target area for Carpinteria flights 3, 4 and 5 shown in the MS image. Ground-level photographs show a closer view of the oil and non-oil features.

The Carpinteria flights took place on June 10, 2021, between 09:30 AM PST and 01:00 PM PST. The weather was calm with winds consistently less than 3 mph. The air temperature ranged between 66° to 71° and the skies were mostly cloud-free and sunny. Five flight missions were performed with the M100 system and two with a smaller, DJI Mavic 2 Enterprise Dual. All the missions at this site were flown at a 20-meter altitude based on a desired resulting pixel size of ~1.3 – 1.4 cm. Three additional data acquisitions were performed with the M100 instrument held at a height of approximately one meter over the large oil patty, each with a different UV filter attached to the JAI-UV lens. These collections were done to assess if a particular wavelength showed any significant advantage to discriminate oil over another. As with McKittrick, the Mavic was flown to provide comparative imagery and to acquire data of a larger geographical area given its longer flight time capability. The same pre-flight procedures followed for the McKittrick flights were performed for each of the Carpinteria flights. Table 4 shows information on each of the data collection missions.

Table 4. Carpinteria flight information

Flight Number	UV Filter (nm)	Air Speed (m/s)	Altitude (meters)	Pixel Size (cm)*	Frame Overlap	Start Time (PST)	End Time (PST)	Duration (min:sec)	Sky Condition	Wind Speed (mph)
1**	365	3.0	20.0	~1.3	75%	09:38 AM	09:48 AM	10:01	sunny, clear	calm (< 3.0 mph)
2	365	3.0	20.0	~1.4	75%	10:20 AM	10:27 AM	06:55	sunny, clear	calm (< 3.0 mph)
3	324	3.0	10.0	~1.4	75%	10:54 AM	11:00 AM	05:55	sunny, clear	calm (< 3.0 mph)
4	324	3.0	30.0	~1.3	75%	11:17 AM	11:24 AM	~07:00	sunny, clear	calm (< 3.0 mph)
5	405	3.0	20.0	~1.3	75%	12:02 PM	12:06 PM	04:35	sunny, clear	calm (< 3.0 mph)
Handheld 1	405	0.0	~1.0	~0.25	N/A	12:19 PM	12:21 PM	~2:00	sunny, clear	calm (< 3.0 mph)
Handheld 2	365	0.0	~1.0	~0.25	N/A	12:23 PM	12:25 PM	~2:00	sunny, clear	calm (< 3.0 mph)
Handheld 3	324	0.0	~1.0	~0.25	N/A	12:26 PM	12:28 PM	~2:00	sunny, clear	calm (< 3.0 mph)
Mavic 1	N/A	***	~61.0	~1.1	75%	12:30 PM	12:36 PM	06:05	sunny, clear	calm (< 3.0 mph)
Mavic 2	N/A	***	~30.5	~1.1	75%	12:37 PM	12:47 PM	10:15	sunny, clear	calm (< 3.0 mph)

\* Size of pixels in the MS image mosaics. The TIR and UV data were subsequently geo-referenced to the MS mosaics and therefore resampled to the same pixel size.

\*\* Location of flight #1 was roughly 50 meters to the east of flights 2-5

\*\*\* Mavic air speed not recorded

The flight plans were designed around the location of the larger oil patty, but to also include variation of substrate and vegetation within the upper intertidal zone. Each flight was pre-preprogrammed as mapping mission grids into the Atlas flight control software with the pilot at the controls in case of emergency and to perform a controlled landing if necessary. A sample flight grid for the Carpinteria site is shown in Figure 7.



Figure 7. Sample flight path over the Carpinteria AOS.

Following each mission, calibration data were collected again for the MicaSense MS camera system using the calibration panel and the rest of the post-flight procedures as outlined above were repeated for each of the seven missions. Photographs and GPS locations of importance were taken over the entire AOS for later reference and use in the assessment of the data quality and accuracy as well as algorithm development. Sample photos are shown in Figure 8.



Figure 8. Sample photos of the Carpinteria AOS and the locations of the target oil patty.

### 3.5 Multispectral Data Processing and Image Mosaicking

The data from the MicaSense MS camera were written to an SD card during data acquisition. Following each flight those data were offloaded onto the USB drive. Data from all the flight USB drives were copied to a Windows-based computer running PIX4D and ERSI ArcGIS Pro. PIX4D uses a camera model for the MicaSense RedEdge camera “rig” (a camera with multiple sensors/lenses) to align the five bands and geospatially orient the data frames for mosaicking (<https://support.pix4d.com/hc/en-us/articles/115005852003-Processing-camera-rigs>). It also matches “key points” in the data frames to determine matching targets to auto-mosaic and orthorectify the datasets. We found that PIX4D generated the most accurate 5-banded mosaic with each band properly aligned with the other bands. For the processing of single data frames alone, however, PIX4D was unable to align the five bands correctly. For this purpose, a Python script was written specific to that task. Another pre-processing application considered was Esri’s Drone2Map application, which integrates Pix4Ds processing capabilities within the ArcGIS software package, however the cost of software licensing did not fit into this projects budget while the month-to-month pricing option with PIX4D did.

As part of the PIX4D processing, the Micasense Red Edge MS data were defined and loaded into Pix4D’s project setup. After setting the project parameters as a 5-banded MS set, PIX4D reads the EXIF header files for each

image, and determines the wavelength and location of each set of frames. MicaSense's data capture best practice requires imaging of a calibration panel at the beginning and end of each flight to adjust for variable lighting conditions during flight. Pix4D recognizes these images and uses it as a calibration image for processing. The default PIX4D 5-band MS project parameters were used. PIX4D processing times ranged from 20 -45 minutes depending on the number of images in a flight. Processing limitations were also dependent on the processing computer hardware, for this project a Windows 10 laptop with the following configuration was used:

- CPU: Intel Core i9-10885H CPU @ 2.40GHz
- RAM: 64GB
- GPU: Intel UHD Graphics, NVIDIA GeForce RTX 2070 with Max-Q Design

When PIX4D processing was complete, the single-banded mosaic of each of the 5 bands was composited using ArcGIS, creating a multispectral 5-banded image which was used in later processing and analyses. The mosaics are of irregular coverage area based on the altitude, flight plan and orthorectification process used by PIX4D.

### **3.6 Thermal Infrared Data Processing and Image Mosaicking**

The data from the TIR camera were written to a different SD card during acquisition. Following each flight those data were offloaded onto the USB drive. Data from all the flight USB drives were also copied to a Windows-based computer running PIX4D and ERSI ArcGIS Pro. For the McKittrick AOS we found that PIX4D generated a geospatially accurate mosaic from the individual data frames. For the Carpinteria datasets however, PIX4D was unable to geospatially correct and orient the data frames to produce an accurate image mosaic. This is because the PIX4D's feature recognition and matching algorithm uses a process to find 'key points' from scene to scene (along with the GPS data) to create the orthomosaics. When a target area is relatively homogenous (e.g., a uniform, sandy beach), the 'relative rig' and feature matching algorithms break down and fail to properly 'stitch' the individual data frames together. It was therefore necessary to manually georeference the TIR data and generate the image mosaics in ArcGIS Pro. Alternate data georeferencing and mosaicking and software was not investigated since the georeference and mosaic process in ArcGIS Pro met the needs of this project. A more reliable application and/or algorithm would be necessary to process at the speeds required for an in-the-field, operational system. Discussion on this follows in later sections. The MS and TIR image mosaics for all eleven flights are in Appendix B.

### **3.7 Ultraviolet Data Processing and Image Mosaicking**

The data from the UV camera were written during data acquisition to a USB drive attached to the SBC. Following each flight, the USB drive was detached cataloged and stored for the post processing. Data from all the UV USB drives were copied to a Windows-based computer running ERSI ArcGIS Pro. Custom software was developed to take the header information from each of the MS frames and build a header file for each of the time-synchronous UV image frames. Then each UV image file was corrected as much as possible for lens-caused image distortion, registered to a WGS-1984 coordinate system and georeferenced to a geospatially accurate image mosaic of multispectral MS data from the same flight. Finally, UV image mosaics were created of the AOS for comparison with the other data sets, UV filter analyses and oil detection algorithm development.

### 3.8 Oil Detection Algorithm Development

One initial hypothesis was that the UV sensor would detect a fluorescence signal from the oil and therefore a combination of UV and MS (visible wavelength) sensors would help isolate the spectral reflectance from oil when compared to the background water and non-oiled, dry substrates and vegetation. Thin oil has stronger reflectivity in the UV than water (oil-1.02, water-0.722) and many solid substrates. Very thin oil sheens of thickness less than 0.1  $\mu\text{m}$  and as thick as 10  $\mu\text{m}$  can be detected using a UV sensor (Grüner, 1991; Klemas, 2010; Goodman, 1994). Past literature has noted that oils of all types from heavy crude to refined fuels also fluoresce when exposed to the UV component of sunlight. Oil will fluoresce at a longer wavelength than the incident radiation. For example, when tar balls are excited with UV radiation at  $\sim 380$  nm, the emitted radiation peaked at  $\sim 430$  nm, and showed detectable intensity into the 500 nm range (Kennicutt, 1983). Through its BSEE-funded work, OI found that emulsified oil shows a higher reflectance in the 324 nm and 365 nm wavelengths than background water and a much higher reflectance intensity than dark, fresh oil. This result was a further indication that a UV sensor would help identify emulsified, weathered oil which is often what reaches the coastal intertidal zone or stream banks after a spill.

This study did not, however, show any significant indication of fluorescence or strong reflectance in the ultraviolet range of the electromagnetic spectrum from the oil targets in either location, nor did the UV filters appear to provide any advantage to isolating an oil-only reflectance signature over the visible or thermal bands provided by the other sensors. What was observed was that sunglint reflecting off the fresher oil was far more apparent in the UV imagery than in the multispectral, visible-to-near infrared data. Sunglint is an optical phenomenon that occurs when sunlight reflects off the surface of a reflective body (most often water) at the same angle that a sensor views it. The result is a mirror-like specular reflection of sunlight off the surface back at the sensor. Previous studies by (Pisano et al.; 2015, Sun and Hu, 2016) have used sunglint to map oil on the ocean's surface, yet sunglint is also often seen as a false positive type of reflective response when trying to detect oil on open water (Fingas and Brown, 2017).

As mentioned above, thin oil sheens on water exhibit high reflectivity in the UV wavelengths, but UV imagery is subject to false positives such as wind slicks, sunglint and biogenic material (Fingas and Brown, 2017). In the dry inland and coastal intertidal environments flown for this study, substrate covered with fresher oil nearly always exhibited strong sunglint when imaged from either a north to south (heading of  $\sim 160^\circ$ ) or west to east (heading  $\sim 90^\circ$ ) - the occurrence of sunglint being more related to flying in the direction of the sun. During the flights at both study sites, the sun azimuth was between  $\sim 92^\circ$  and  $\sim 240^\circ$ . The sUAS cameras tilted forward in flight due to a slight upward pitch of the aircraft. The oil appeared almost black (very low reflectance) when the sUAS was flying over the targets in the opposite direction. The result was sunglint readily apparent emanating off the oil and oiled substrate when using any of the three UV filters (Figure 9). While the use of sunglint as a means to detect and classify potential oil targets as part of reconnaissance cannot be ruled out entirely, the UV data were ultimately not used in the algorithm to detect oil. The use of a UV sensor is discussed below as a possible supplementary device toward that objective.

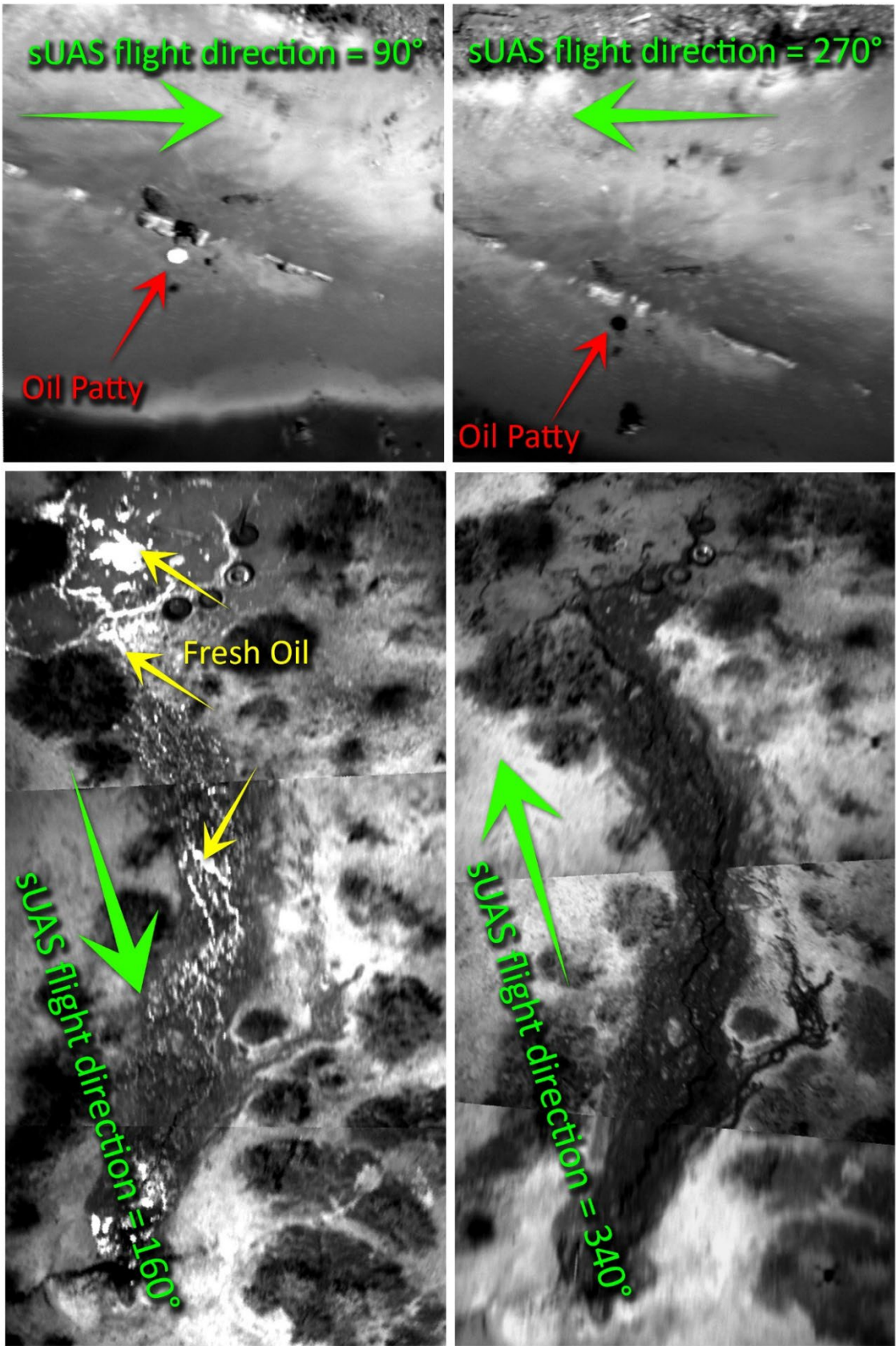


Figure 9. UV Sunglint examples from both study sites.

The sensors determined to be the most effective at detecting and mapping high probability oil targets for SCAT teams and general reconnaissance are a combination of the MS and TIR cameras especially the red edge channel on the MicaSense. In both the McKittrick and Carpinteria data sets the fresher oil had a very low reflectance (high absorption) in the red edge channel compared to almost all other non-oiled, wet and dry vegetation and substrates. In addition, the reflectance from most non-oiled materials compared to that of oil showed a lower signal intensity in the red, green and blue channels compared to both the red edge and near infrared bands. This intensity divergence combined with the high reflectance in the thermal infrared (higher emissivity) of the fresher oil versus the relatively lower reflectance (lower emissivity) from most of the other targets allowed for the creation of a band combination algorithm that effectively identified areas with a high probability of oiling.

The algorithm proving to be effective on all the datasets from both study sites is a multi-step process:

1. Geospatially co-register the MS and the TIR image mosaics to each other using the highest resolution data set as the master. In this case the TIR data were co-registered to the MS data, super sampling the TIR data to match the cell size of the MS data.
2. Clip both the TIR and MS co-registered image mosaics to the smallest geographical extent to exclude any area which does not contain usable data from both the MS and TIR data.
3. Run the 5-banded multispectral image composite through a band ratio equation generating a single-banded image file in which the oiled pixels show a high digital number relative to non-oil pixels.
4. Apply a predetermined histogram threshold cutoff to generate a single-class image showing high probability oiled pixels.
5. Using the MS mosaic as input, create a single banded image file using the Soil Adjusted Vegetation Index (SAVI).
6. Apply a predetermined histogram threshold to generate a single-class image used to mask out non-oiled pixels in the output from step four. This mask effectively helps to mask out non-oiled vegetation and substrate that reflect strongly in the red edge and near infrared (NIR) wavelengths.
7. Generate a second mask by applying a histogram cutoff in the co-registered TIR data. Apply the mask to the output of step six.
8. Generate GIS/COP-ready products from this process.

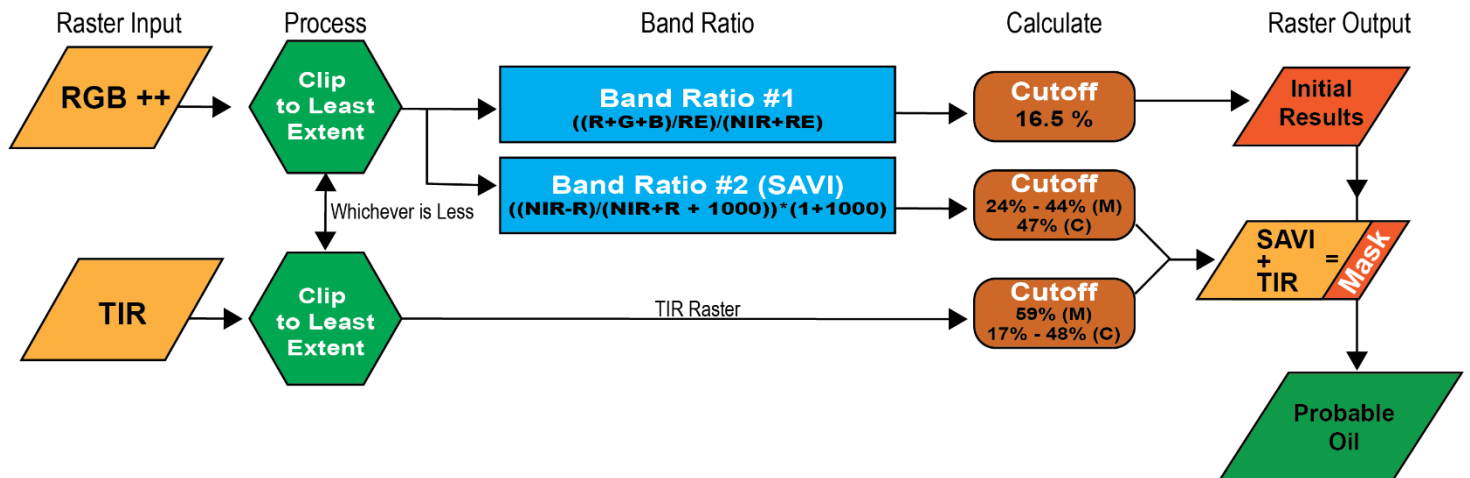


Figure 10: Algorithm / Processing flow chart. Histogram threshold cutoff differed for the SAVI and TIR masks between the two study sites (M=McKittrick and C=Carpinteria). Further explanation on these cutoffs and the mask follows in the SAVI Mask and TIR Mask sections.

### 3.9 Multispectral Oil Extraction Equation

The creation of the primary data product developed in step three above is used as the base image for the final oil identification map. The image is generated using the MS data and a simple equation that takes advantage of two reflectance characteristics of oil (and oiled material) along with non-oiled substrate and vegetation. First, heavy to light crude oils exhibit a relatively low reflectance intensity in the visible to NIR range of the spectrum compared to soil, sand, vegetation and water (Svejkovsky, 2012, Allen and Krekeler, 2010). Second, the reflectance of most of the vegetation types, soil and sand in our study areas increased in the red edge and NIR bands. Figures 11A and 11B show representative MS and TIR image data and the reflectance intensities as digital numbers along a transect line in each of the data sets for the two AOS.

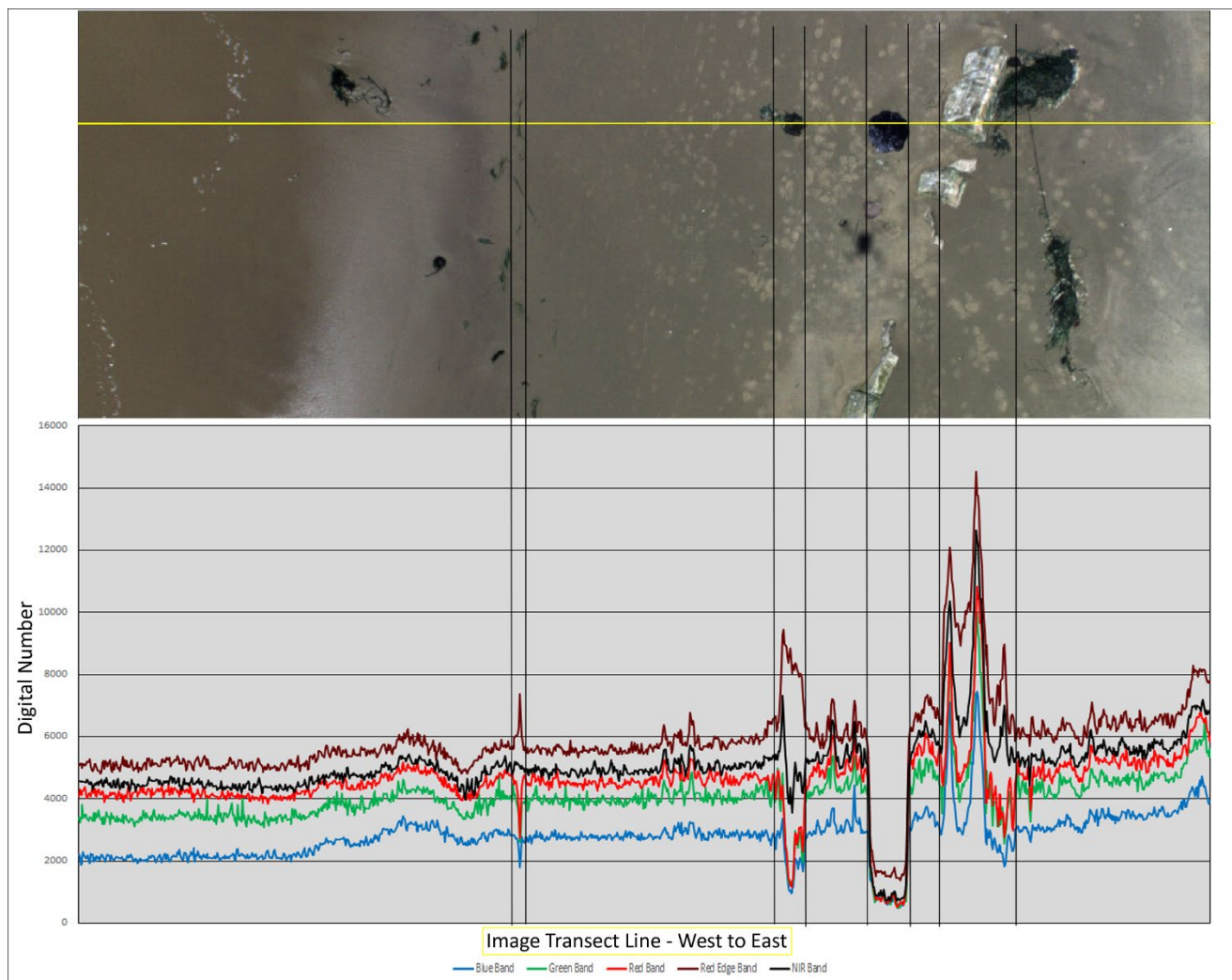


Figure 11A. Section of the Carpinteria AOS showing different substrates, vegetation and the oil patty target as imaged by the MicaSense MS camera using the bands described in Table 2 above. Bottom graph shows the digital number profiles for each of the red, green, blue, red edge and near infrared bands along the yellow transect line in the imagery. The vertical lines are shown to simplify reference of areas along the transect graph where the reflectance decreases to almost zero in all bands (oil patty) and where there is a divergence between the reflectance intensities in the red edge and near infrared bands and the red, green and blue bands (vegetative beach wrack).

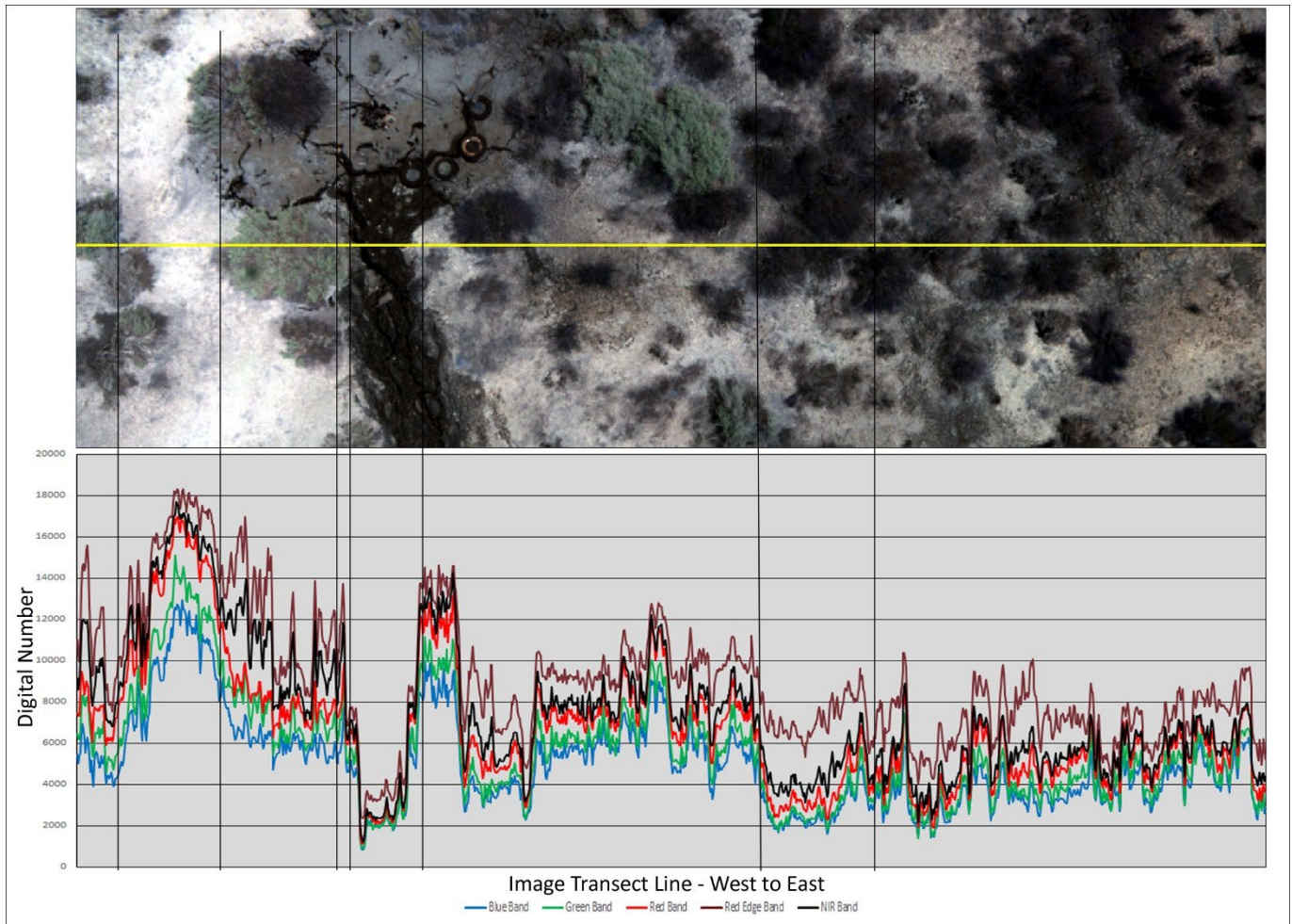


Figure 11B. Section of the McKittrick AOS showing different substrates, vegetation and the oil seepage target as imaged by the MicaSense MS camera using the bands described in Table 2 above. Bottom graph shows the digital number profiles for each of the red, green, blue, red edge and near infrared bands along the yellow transect line in the imagery. The vertical lines are shown to simplify reference of areas along the transect graph where the reflectance decreases to low levels zero in all bands (oil seep area) and where there is a divergence between the reflectance intensities in the red edge and near infrared bands and the red, green and blue bands (both greener and darker vegetation as well as an area of bare ground).

The depressed reflectance of oil in the red edge and NIR wavelengths and the increased reflectance intensities of different substrate and vegetation in these wavelengths provides a foundation for the equation below. The multiband ratio generates an image in which the digital numbers for pixels containing oil and oil-covered material are effectively magnified in relation to non-oiled material.

$$\frac{((\text{Red} + \text{Green} + \text{Blue}) / \text{Red Edge})}{(\text{Red Edge} + \text{NIR})} \quad \text{or} \quad \frac{((\text{Band 1} + \text{Band 2} + \text{Band 3}) / \text{Band 4})}{(\text{Band 4} + \text{Band 5})}$$

A histogram threshold cutoff of 16.5% for the McKittrick and Carpinteria AOS was determined to be the best balance between the identification of known oiled pixels and reducing the number of false positive pixels (pixels known to be not oil but showing a high digital number in the resultant products). The cutoff was applied to all the files generated by this first step to produce the base images from all eleven flights for the final oil vs. nonoil classification.

### 3.10 SAVI Mask

The next step in the process is to generate an image file to mask out as much non-oiled vegetation as possible. Several variations of vegetation index equations were tested on the MS data from both AOS. The SAVI version of the index was found to be the most effective in masking out vegetation that was missed (identified as a false positive for oil) by the first step. SAVI is used to correct Normalized Difference Vegetation Index (NDVI) for the influence of soil brightness in areas where vegetative cover is low (USGS, 2021). Both study sites either had low levels of vegetation or vegetation that showed low levels of vigor (high reflectance in the green wavelengths). The SAVI band equation is normally expressed as the ratio between the Red and NIR values with a soil brightness correction factor (L) defined as 0.5 to accommodate most land cover types.

$$((\text{NIR} - \text{Red}) / (\text{NIR} + \text{Red} + L)) * (1 + L)$$

For this study the SAVI equation was modified to account for the digital numbers in the MS data mosaics and to mask as much vegetation as possible without including oil and oiled material. The modified SAVI equation used to generate the first mask was therefore:

$$((\text{NIR} - \text{Red}) / (\text{NIR} + \text{Red} + 1000)) * (1 + 1000)$$

A histogram threshold cutoff of 47% +/-1% was applied to the result of the SAVI equation performed on the Carpinteria data to generate the first false positive mask. For the McKittrick image products a standardized cutoff could not be applied without over or under masking the high probability oiled areas. Histogram cutoffs between 24% and 44% were used depending on the flight. This lack of uniformity in the SAVI result from the McKittrick data was most likely due to the significant differences in flight coverage areas and altitudes flown in combination with the change in sun angle between the different flights. This mask was combined with the product of the initial oil identification process to produce an image in which more of the false positives are eliminated. It was then passed on to the next step in the processing procedure.

### 3.11 TIR Mask

The final step in the procedure is to use the TIR data to further distinguish the oil and oiled material from all else. The TIR mask uses the higher emissivity of thick oil in relation to much of the non-oiled material to further remove non-oiled pixels which remained through the first two steps as false positives. Thin oil films (~ < 10-20 um) are typically undetectable using a thermal sensor imaging in the 7500 – 13,500 nm wavelength range. Thicker but still relatively thin oils up to ~70 um are detectable but show lower emissivity than water and vegetation and so appear cool. Petroleum substances thicker than ~70 um (and darker) tend to trap and re-emit solar heat input and thus appear warmer than water during the day (Svejkovsky, 2012). In the case of the two environments imaged for this study the vegetation and sand (both wet and dry) emitted cooler temperatures than the oil targets.

This third mask works to preserve the probable oil and oiled material, but eliminate a few more known non-oil, false targets from the final product. A thermal histogram cutoff of 59% was used to generate the final non-oil mask for the McKittrick data sets, however a standardized percent cutoff could not be applied universally across the TIR data from Carpinteria. The percent cutoffs used to create the best mask from the Carpinteria TIR data ranged from 17% to 48%. This variability was necessary because to the low quality of the thermal imagery mosaics generated from the Carpinteria flights. Since PIX4D was unable to generate usable TIR mage mosaics for this AOS, the mosaics had to be created manually using ArcGIS. One notable drawback is that the Zenmuse XT camera has a stated accuracy of +/- 10.0°C which is relatively imprecise when compared to other TIR cameras. The lack of precision resulted in thermal image mosaics displaying high variability from scene to scene and flight line to flight line. This variability in the Carpinteria data led to the mask being less effective at discriminating oil from other targets.

The result of the multi-step process is a GIS-compatible thematic map showing high probability oiled areas. Figures 12a and 12b shows the sequence of images and derived products in the processing sequence for one of the McKittrick and one from Carpinteria.

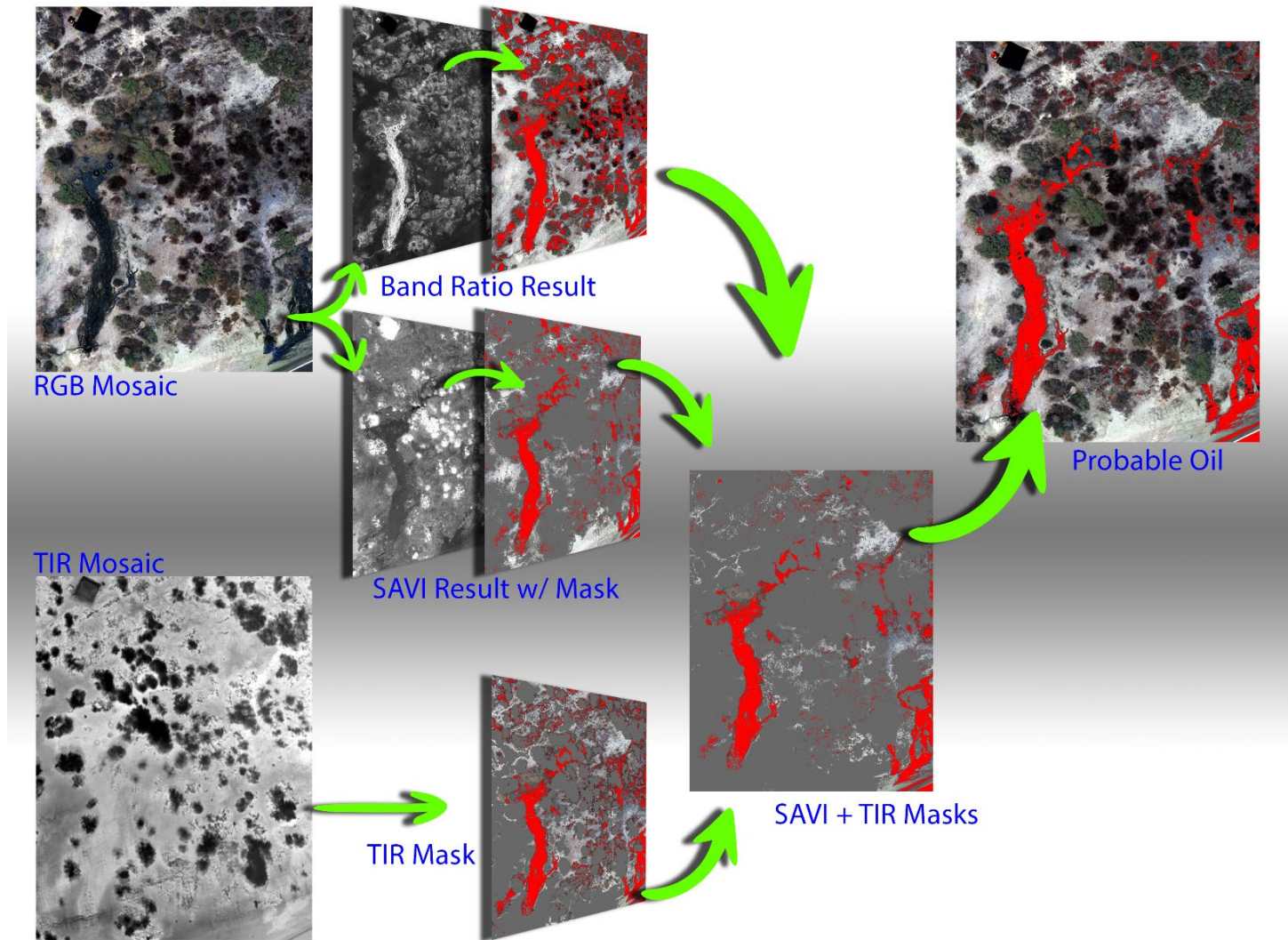


Figure 12a. The algorithm processing step sequence and the example resulting image products for the McKittrick site.

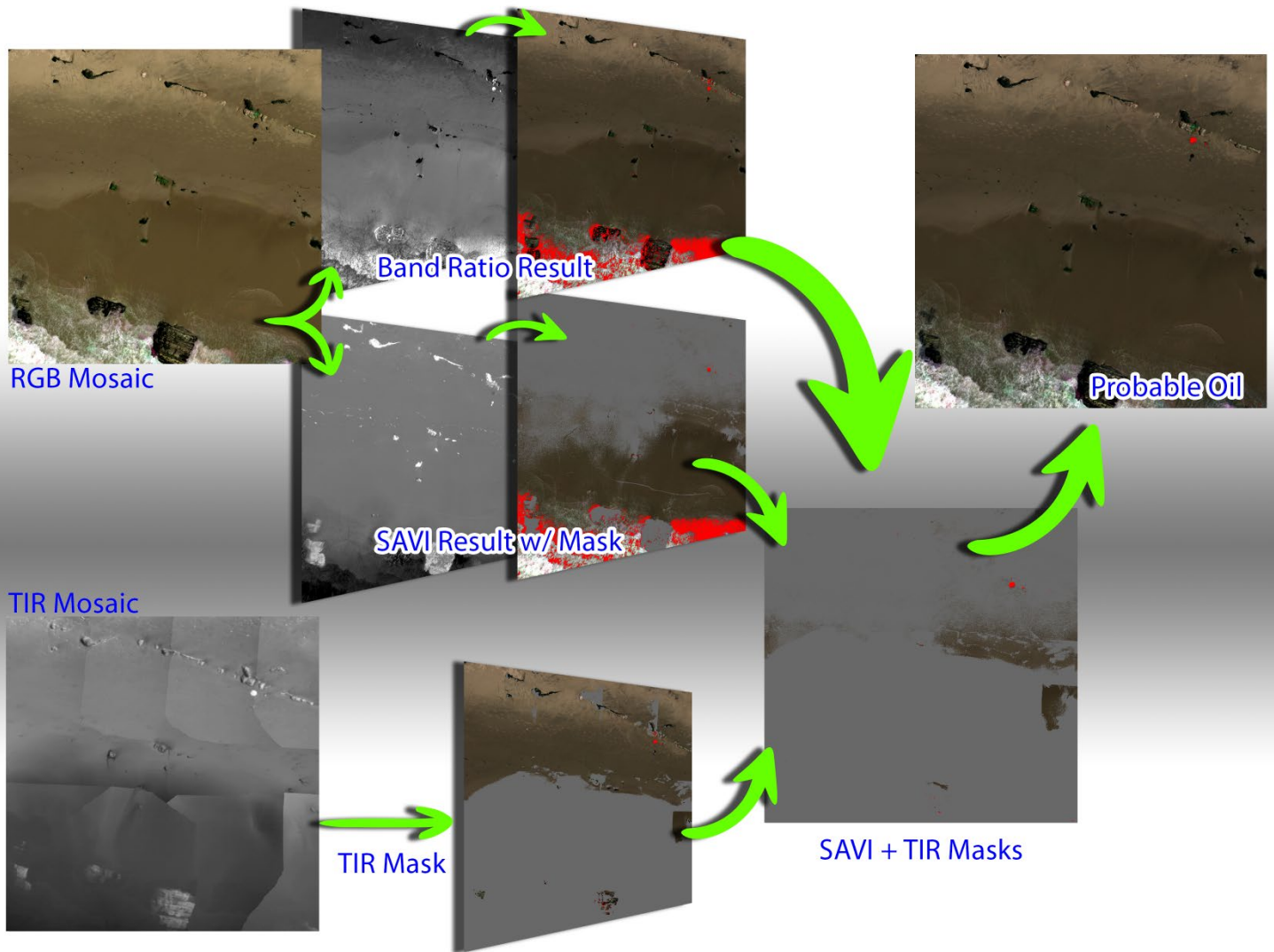


Figure 12b. Figure 12a. The algorithm processing step sequence and the example resulting image products for the Carpinteria site.

## 4.0 Results

### 4.1 Oil Identification Using UV

Since the oil did not show any significant reflection intensity or fluorescence in the UV using any of the three filters, data from the UV camera was not included in the final oil detection algorithm. Despite the results, this does not entirely preclude the use of a UV sensor, or perhaps a sensor imaging in the low 400 nm blue to violet range, for inland and coastal oil detection. The sunglint was just as apparent when imaging with the 405 nm filter. Instead of including a higher functioning UV camera (compared to the JAI UV camera) in a final operational system, the more practical and cost-effective option would be a multispectral camera system that uses an interference filter in the low 400 nm range. Figure 13 illustrates how a combination of sensors imaging in the violet to UV range and TIR could be used to produce a map showing high probability oiled areas.

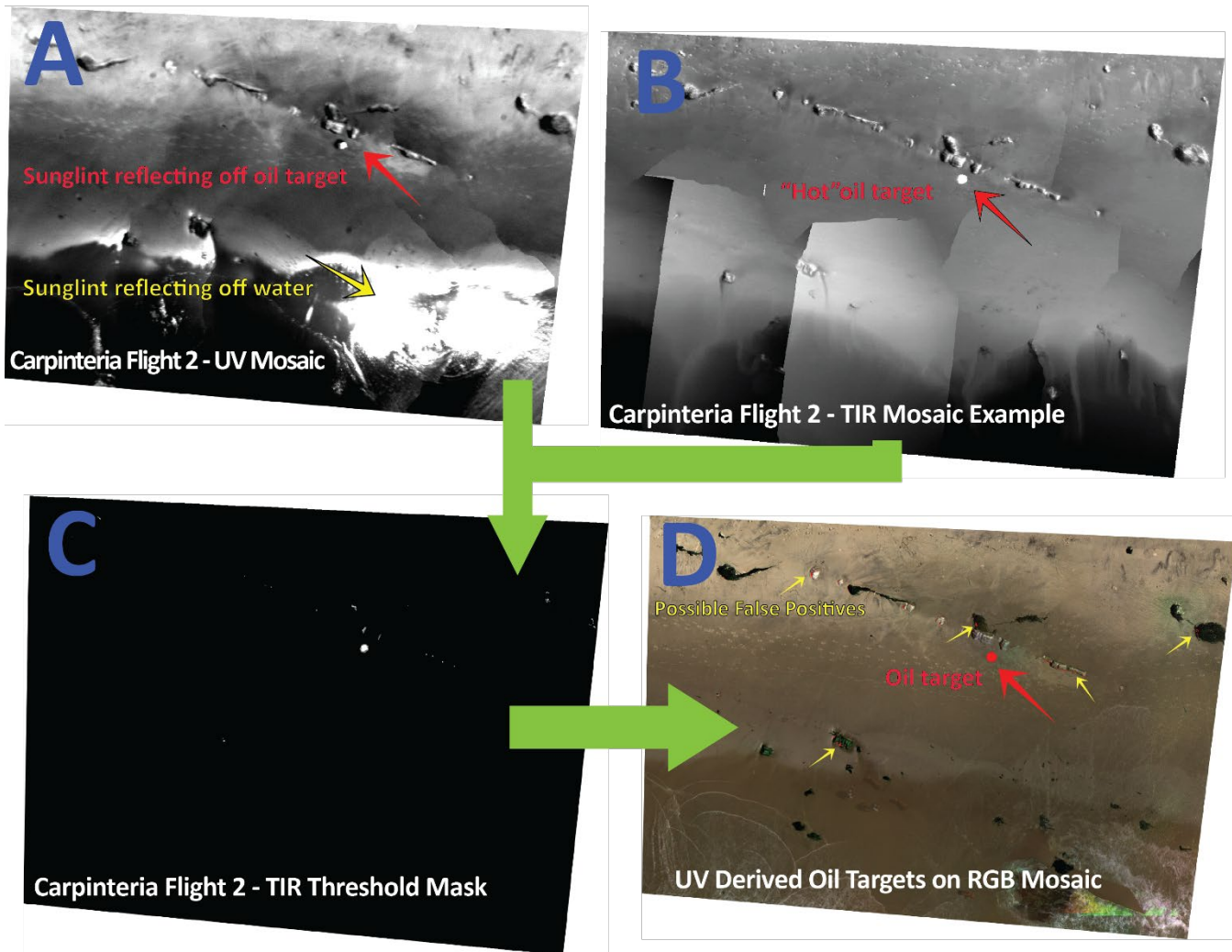


Figure 13. Sample oil identification product derived from UV (A) and TIR (B) imagery acquired during flight #2 at the Carpinteria site. First, the sunglint is isolated in the UV image (A). Next, a temperature threshold mask (C) is created using the co-registered TIR data (B). Finally, the mask is used to extract the possible oil and overlaid on the matching RGB mosaic (D).

## 4.2 Oil Identification Using MS and TIR

Red-Green-Blue image composites, TIR imagery and the resulting oil probability maps for the eleven flights completed at McKittrick and Carpinteria are provided in Appendix B. The algorithm outlined on pages 19-24 using data from the 5-channel multispectral camera combined with that from the TIR camera proved to successfully detect and visually isolate oil and oiled substrate with a relatively small percentage of possible false positives. Budget and time did not allow for the rigorous and precise field work necessary to fully determine the exact location of every oil seep and patch in the entire McKittrick AOS. Thorough review of the many field photos, knowledge of the AOS and close examination of all the MS and TIR data resulted an estimate that the binary oil-non-oil classification product for the McKittrick AOS is between 75%-85% accurate for the six overflights performed. In this case, accuracy is defined as the ability to detect all oiled areas in the AOS while showing the least number of false positives for oil identification. Some potential false targets in the McKittrick AOS were the asphalt road, old tires and wood planks in the main seep area. While the algorithm did classify parts these targets as “high probability oil”, this was more likely due to the residue of oil covering the targets. The tires and some wood planks showed patches covered with well-weathered tar, though the amount oiling over time was difficult to quantify. The road had oil seeping out of the surface and therefore was also classified as oil. Fortunately, a road would not be a difficult area for SCAT teams to visually survey and so this type of false positive is not concerning.

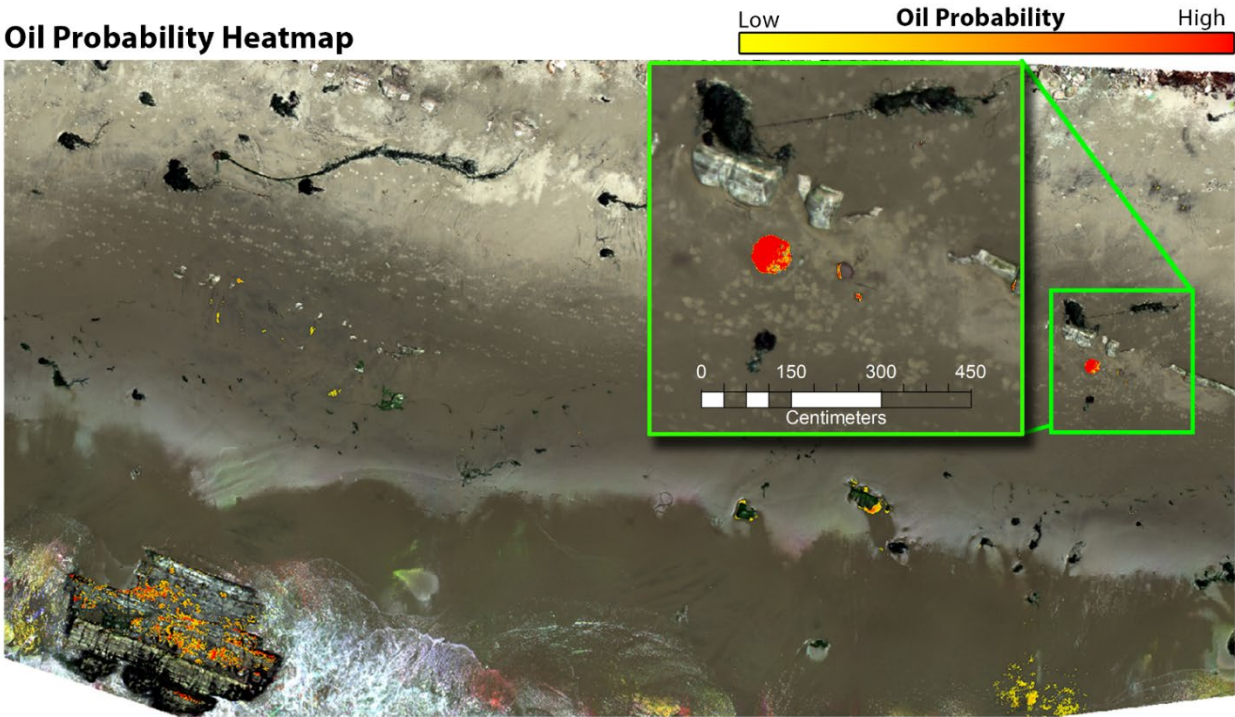
Since there was very little fresh oil and only a few well-weathered tar balls within the intertidal zone at the Carpinteria site the estimate of accuracy is higher. The algorithm was closer to 90% effective at discriminating oil from non-oiled substrate and vegetation. Not only was the system and algorithm able to isolate the larger oil patty with 100% confidence, the exposed section of the tar ball, patch of oil mixed with sand and the smaller oil droplets (measured to be ~ 4 cm x 4 cm in size) were also correctly identified in all the flights.

Another promising result was that the algorithm was able to mostly rule out the warm, dark rocks covered in both flora and fauna in the southern sections of the AOS as being a high probability oil targets. Historically, discriminating oil from dark, rocks and substrate with high thermal variability in the intertidal zone has been a challenging task. For most flights, only few small spots on these rocks were flagged as oil by the algorithm. As a future development to account for the existence of possible false positives, a GIS-ready oil probability 'heat map' could be produced to convey the level of confidence in the oil identification. As seen in the samples in Figure 14, the 'oil' features in a single-class product on the dark rocks in the lower intertidal zone would be represented as having a low to mid-level of confidence of being oil in a heat map style product (Figure 14a). Probable false positives in the unoiled brush in the McKittrick AOS with low confidence of being oil are also depicted as such (Figure 14b).

# Oil Probability Using Heatmap vs. Single Class Oil Product

## Carpinteria Bluffs, sUAS Flight 5

Oil Probability Heatmap



Oil Probability -Single Class

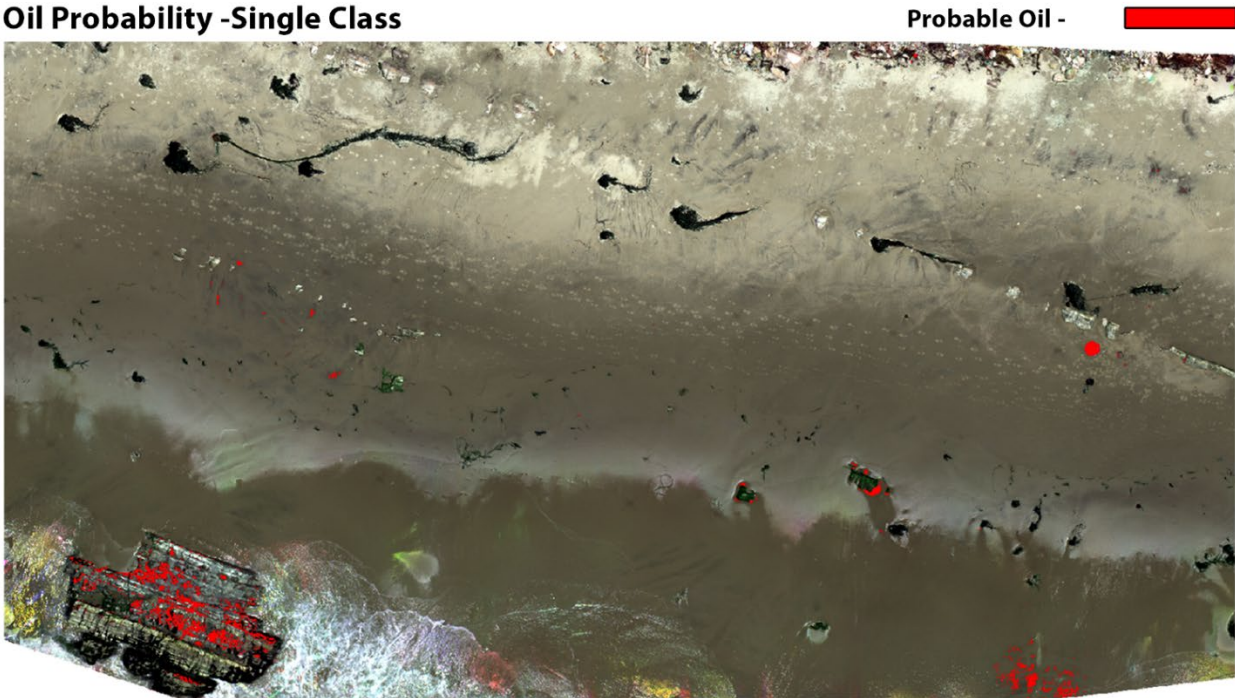


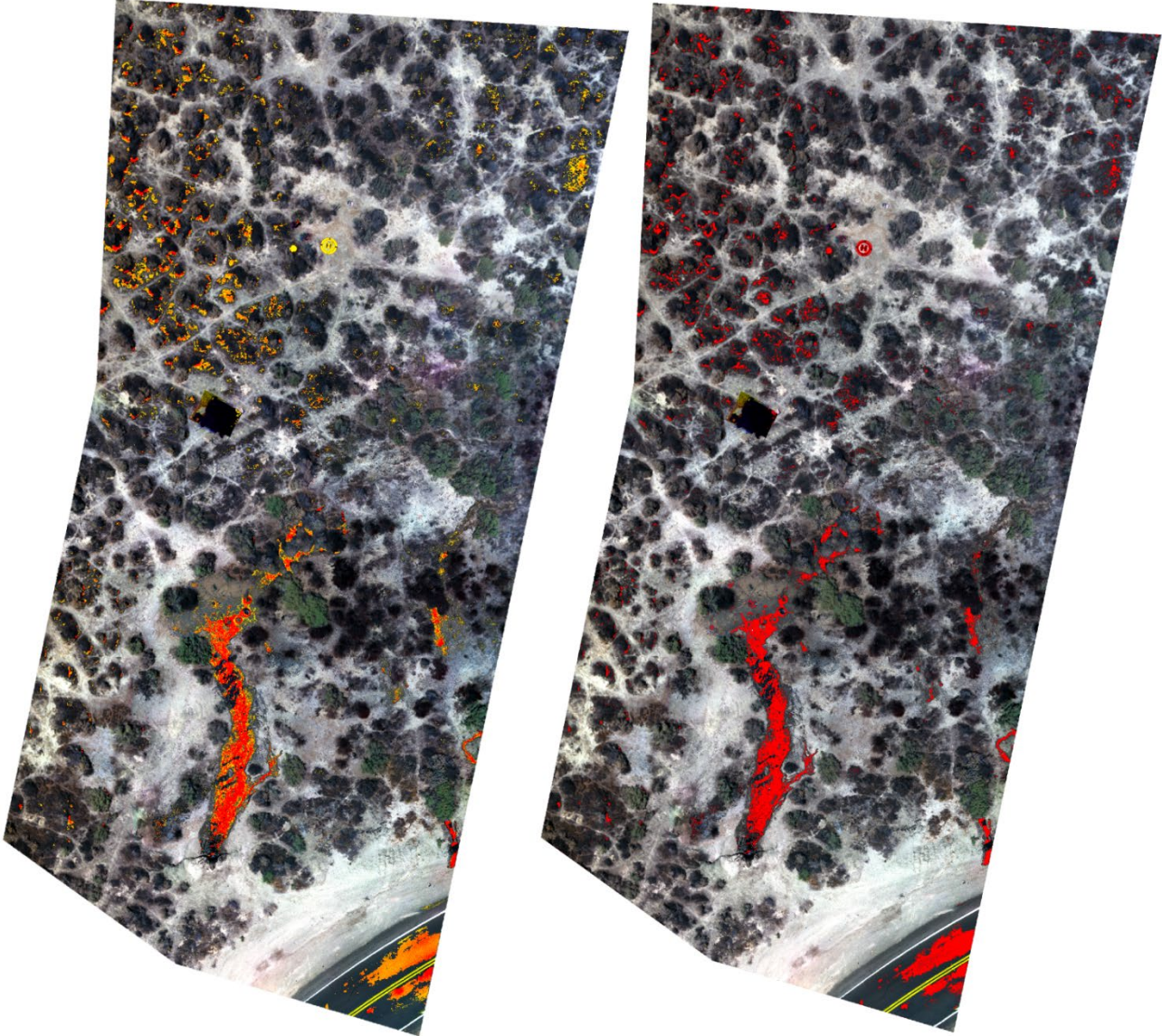
Figure 14a. Example heat map style oil probability product for the Carpinteria.

# Oil Probability Using Heatmap vs. Single Class Oil Product

McKittrick Oil Fields, sUAS Flight 5

Oil Probability Heatmap

Oil Probability -Single Class



Low **Oil Probability** High

Probable Oil -

Figure 14b. Example heat map style oil probability product for the McKittrick site.

In the ideal oil detection method, each step in the process (band ratio output, SAVI mask and TIR mask) would have set histogram cutoff percentages which could be used regardless of the environment, lighting, weather, altitude, or direction of flight, etc. A fixed percent threshold cutoff (16.5%) was used on the band ratio output images. Unfortunately, this project's process did require some adjusting of histogram cutoff values between the study sites for the SAVI and TIR masks. The variation in the percent histogram cut-off thresholds applied to the resultant masks (SAVI false positive mask for the McKittrick data and TIR false positive mask for the Carpinteria data) were likely more related to data quality and controllable factors dealing with flight planning than a flaw in the process. A possible modification to the process could be the incorporation of lookup tables that apply different cutoffs based on environment type and conditions at the time of the survey. Additional solutions based on equipment enhancements are presented in the Discussion section below.

The smallest size of an identifiable oil target was estimated to be approximately 4cm x 4cm. This was determined computing the average size of the smallest oil globules correctly identified as oil on the Carpinteria Beach. Figure 15 as well as the classification products in Appendix B show the small droplets of oil that the algorithm was able to correctly detect and isolate from the background substrate.

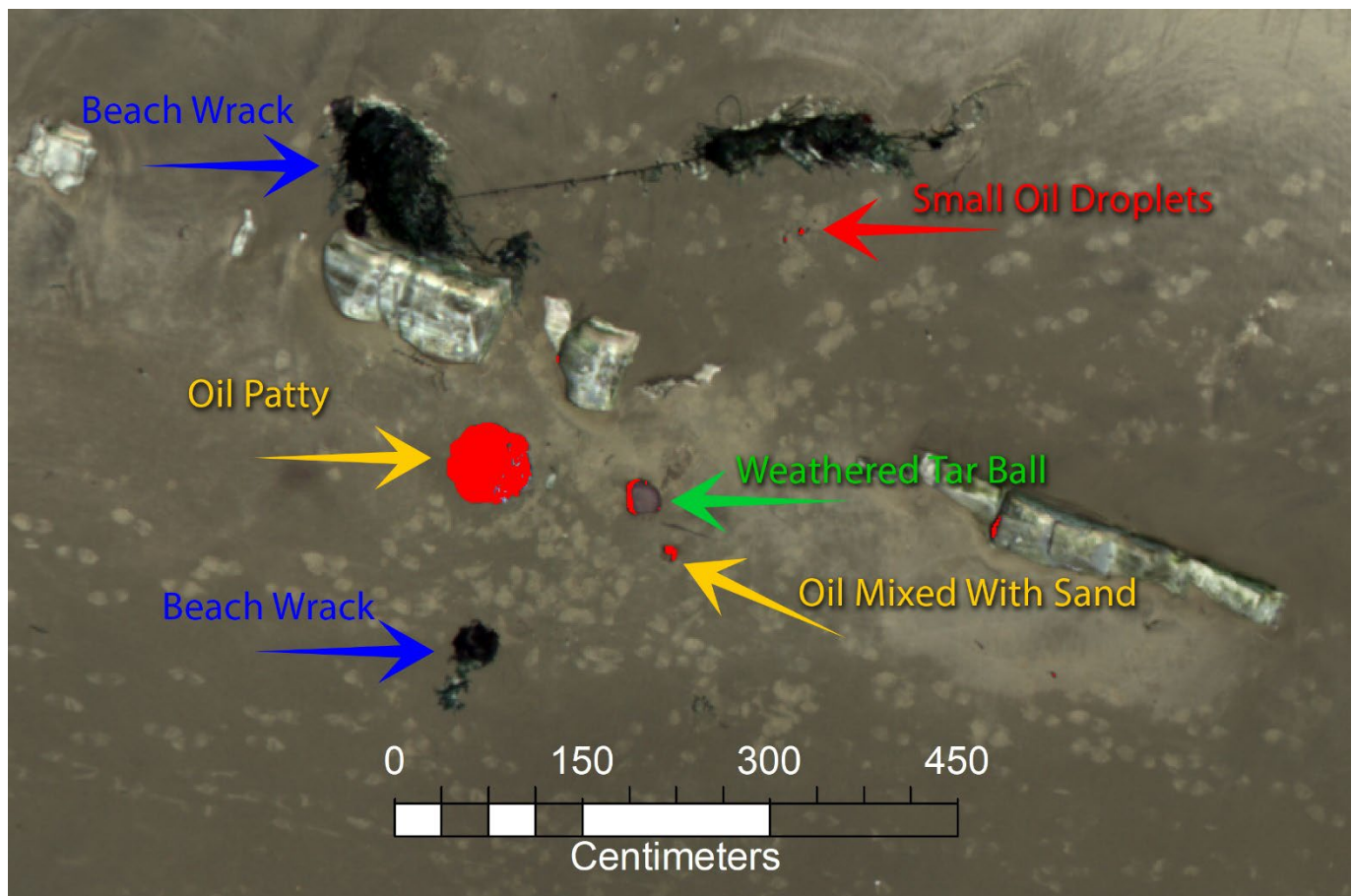


Figure 15. Expanded view of the probable oil product derived from the MS and TIR data acquired on flight 5 at the Carpinteria site. The small droplets of shown are roughly 4 cm x 4cm in size.

Due to the very high spatial resolution of the MS and TIR data (between 1.1 cm and 2.5 cm depending on flight altitude) and the absence of comparison GPS data or imagery with spatial resolution higher than 1 meter, a precise positional accuracy for the imagery and resulting oil probability maps was difficult to quantify. A RTK GPS unit was not available for loan nor in the budget to purchase for this project. GPS readings were collected of the oil targets and the M100 landing pad, but with an accuracy no better than 1 meter. The Esri base layer imagery also only has an accuracy of +/- 1-meter CE90. Once processed through the PIX4D band alignment and mosaicking routine, the GPS data obtained was used in tandem with Esri base imagery to generate products with a horizontal accuracy of +/- 1-meter CE90 for the MS and TIR imagery.

## 5.0 Discussion

The results show that a 5-channel multispectral camera (with one channel imaging in the lower 700 nm, red edge range) combined with a TIR camera imaging system could provide sufficient oil identification to aid SCAT and other response workers. While identifying oil with 100% accuracy and confidence was not possible, this metric was not the goal of the project nor is it necessary for a SCAT reconnaissance tool. If near-100% identification accuracy would be required, for example if mapping oil in a sensitive habitat as part of Natural Resource Damage Assessment (NRDA) work, ground truth data could be acquired to help get closer to that standard. Designing and building a relatively low cost, highly portable, operational sUAS-based system that identifies high probability oiled areas without immediate field verification is achievable. sUAS are relatively easy to operate and flight plan design and control applications are constantly improving. Thus, preparing and implementing scouting missions for difficult to reach areas would require minutes when using an sUAS-based system rather than hours. Even at higher altitudes flown to cover more area per flight, the ability to locate oil and oil-covered material at the centimeter scale is attainable.

### 5.1 Further Research and Algorithm Refinement

Additional research and development is necessary to produce an operational system that is cost effective, relatively simple to operate, and more accurately identifies different oil types and states in multiple environments.

Work should be done to assess how the equipment and algorithm perform on oil emulsions. The oil imaged at the McKittrick site likely had a very low percentage of entrained water, if any. The oil was highly weathered in areas, but not emulsified. The fresher oil on the beach in Carpinteria no doubt had a percentage of entrained water but was not in an emulsified state. In many cases, emulsified oil from a spill or leak will be found washed up on a shoreline (coastal and inland). Researching a methodology to assess how the equipment and algorithm perform on oil emulsions will increase the overall accuracy of the system.

There is also a need to acquire data of oil and oiled material in more habitats under different lighting conditions (i.e., cloud-covered skies). This expanded research will focus the algorithm and help to build a segment of the threshold lookup tables to be applied during each processing step when working in specific environments. Such a database could also be used in a random forest type of learning algorithm to help automate the detection and mapping process.

A future project that budgeted more time and funding for more detailed field work would also serve to improve the overall accuracy of the oil probability maps. Accuracy assessment methods such as a Congalton matrix (Congalton, 2019) could be implemented to increase the overall confidence in the information delivered to the end user.

A more capable sUAS platform with higher spatial and thermal resolution sensors such as those described in the next section could be developed to provide superior functionality such as precise, simultaneous data acquisition,

real time streaming of data from multiple sensors at once, real time GPS-derived location information and easy co-registration of the different image data sets for faster processing.

The most effective system would generate GIS-compatible thematic maps of high probability oiled areas relatively quickly in the field with as little operator intervention as possible. The products should then be easily disseminated to SCAT teams, other response personnel and a common operational picture such as NOAA's Environmental Response Management Application (ERMA). More streamlined and pre-packaged functionality would be necessary to achieve this goal. Ideally the sUAS would include an inexpensive onboard SBC to process the MS and TIR image frames in-flight, apply the oil detection algorithm as a visual filter and stream down the oil probability map to the operator's controller interface in real time. Further research would help to refine the algorithm histogram threshold cutoff for each step in the process. Interactive, selectable oil detection and masking cutoffs could be added to operator interface to improve oil detection and visualization capability in different environments. The enhanced could also serve as a multi-utility tool capable of flying many other different types of missions such as habitat mapping, animal mapping/enumeration, kelp mapping as well as search and rescue. Application-specific algorithms could be developed to quickly detect and classify other targets such as oiled animals.

## 5.2 Proposed Operational System

The DJI Matrice 100 platform and cameras used for this project fit the purpose and budget of the study but are not suitable for an operational system. As discussed above, the DJI M100 platform along with the N1 controller were not capable of controlling more than one camera. Also, the JAI UV and Zenmuse TIR cameras did not integrate easily with the DJI platform. More importantly, at the time of writing this report, neither the DJI M100, the JAI CM-140GE nor the Zenmuse XT are in production. The MicaSense RedEdge-M has also been replaced with the RedEdge-P, RedEdge-MX, RedEdge-MX Blue and the Altum. Depending on government regulations DJI is still the most capable platform to consider. The DJI M 300 RTK is the latest enterprise-level drone that is well-suited for this application. The current cost of this unit ranges from \$12,000 - \$16,000 depending on configuration.

The MicaSense Altum provides 5-channel data as the RedEdge-M, yet the CCDs are of a higher resolution (2064 x 1544 pixels compared to 1280 x 960). The Altum also incorporates a TIR camera which operates seamlessly with the multispectral outputting scenes that are temporally and geospatially in sync. The shortfall, however, is that the TIR sensor is extremely low resolution at 160 x 120 pixels. While the TIR data can be super-sampled in post processing to match the coverage area of the MS data, the GSD of the resulting TIR image data (when composited) would most likely be unusable in the algorithm developed via this study. The solution would be to add a second, higher resolution (both thermally and spatially) TIR camera. The successor to the Zenmuse XT is the Zenmuse H2OT. This camera has a 20 MP zoom camera and a 12 MP wide angle camera integrated with the 640 x 512 resolution TIR sensor (excess functionality for this application) but is currently all that is available to operate seamlessly on the DJI M300 platform. Even though the Zenmuse XT is no longer in production, it can still be purchased, but at a price only a few hundred dollars less than the H2OT. Although the stated thermal accuracy of the Zenmuse H2OT is much higher (+/- 2.0°C) than that of the XT (+/- 10.0°C), +/- 2.0°C is not competitive compared to other thermal sensors on the market. Finding a lighter weight, sUAS-compatible TIR sensor would significantly improve the effectiveness of the TIR mask. The cost of the M300-MicaSense Altum combination is approximately \$27,000 at the time of this report. The addition of the Zenmuse H2OT would bring the total hardware cost to between \$38,000 - \$40,000. Since the latest DJI flight controller software facilitates the data acquisition, storage and streaming for multiple cameras (unlike the M100/N1 combination), developing software to acquire and co-register the MS and TIR data for the purpose of applying the procedure described here would be relatively inexpensive.

## References

- Allen, C. & Krekeler, Mark. (2010). Reflectance spectra of crude oils and refined petroleum products on a variety of common substrates. Proceedings of SPIE - The International Society for Optical Engineering. 7687. 10.1117/12.852200.
- "California Air Resources Board." *LCFS Crude Oil Life Cycle Assessment | California Air Resources Board*, <https://ww2.arb.ca.gov/resources/documents/lcfs-crude-oil-life-cycle-assessment>.
- Congalton, Russell G., and Kass Green. Assessing the Accuracy of Remotely Sensed Data: Principles and Practices. CRC Press, 2019.
- Fingas, Merv, and Carl Brown. "A Review of Oil Spill Remote Sensing." *Sensors*, vol. 18, no. 2, 2017, p. 91., doi:10.3390/s18010091.
- Goodman, Ron. "Overview and Future Trends in Oil Spill Remote Sensing." *Spill Science & Technology Bulletin*, vol. 1, no. 1, 1994, pp. 11–21., doi:10.1016/1353-2561(94)90004-3.
- Grüner K., Reuter R., Smid H. A New Sensor System for Airborne Measurements of Maritime Pollution and of Hydrographic Parameters. *Geojournal*. 1991;24.1:103–117.
- Kennicutt, Mahlon C., and James M. Brooks. "Relationship between Pelagic Tar, Fluorescence and Biological Markers in the South Atlantic Ocean." *Marine Pollution Bulletin*, vol. 14, no. 9, 1983, pp. 335–342., doi:10.1016/0025-326x(83)90394-6.
- Klemas, Victor. Tracking Oil Slicks and Predicting their Trajectories Using Remote Sensors and Models: Case Studies of the Sea Princess and Deepwater Horizon Oil Spills. *Journal of Coastal Research: Volume 26, Issue 5, 2010*, pp. 789 – 797.
- "Landsat Surface Reflectance-Derived Spectral Indices." *Landsat Soil Adjusted Vegetation Index*, <https://www.usgs.gov/core-science-systems/nli/landsat/landsat>
- Pisano A, Bignami F, Santoleri R. Oil Spill Detection in Glint-Contaminated Near-Infrared MODIS Imagery. *Remote Sensing*. 2015; 7(1):1112-1134. <https://doi.org/10.3390/rs70101112>
- Sun, Shaojie and Hu, Chuanmin, "Sun Glint Requirement for the Remote Detection of Surface Oil Films" (2016). C-IMAGE Publications. 74. [https://scholarcommons.usf.edu/cimage\\_pubs/74](https://scholarcommons.usf.edu/cimage_pubs/74)
- Svejkovsky J., W. Lehr, J. Muskat, G. Graettinger and J. Mullin. 2012. Operational utilization of aerial remote sensing during oil spill response: Lessons learned during the Deepwater Horizon spill. *Photogrammetric Engineering & Remote Sensing*, 78(10), pp. 1089-1102.
- "Zenmuse H20 Series - FAQ - Dji." *DJI Official*, [Zenmuse H20 Series - FAQ - DJI](#)
- Zenmuse XT User Manual - *Dl.djicdn.com*.  
[Zenmuse XT User Manual V1.2 en 0708.pdf \(djicdn.com\)](#)

## Appendix A: Equipment Inventory

- 1) DJI M100 Platform
- 1) DJI Flight Controller (Model GL658C)
- 2) DJI Intelligent Flight Batteries (TB48D)
- 1) DJI AC Adapter (Model A14-100P1A)
- 1) Zenmuse XT 30HZ V2 13mm
- 1) Zenmuse XT Gimbal set VR2 (attached to M-100)
- 1) MicaSense RedEdge-M Multispectral camera (attached to M-100 and operational)
- 1) UKA Optics C-Mount 6mm UV Lens, 30.5mm
- 1) UV Bandpass Filter BP324.-30.5/30.5mm
- 1) UV Bandpass Filter BP365.-30.5/30.5mm
- 1) Blue Interference Bypass filter Bi405/30.5mm
- 1) JAI CM-140GE UV Camera
- 1) JAI 2-meter power cable 12pin
- 1) JAI Tripod Adapter/MP-40
- 1) Basler Cable Gig E CAT6 5m/A1
- 1) Power harness and associated Hirose cables for SBC and JAI-UV camera
- 1) Raspberry SC15184 Pi 4 Model B 2019, Quad Core, 64-Bit, Wi-Fi, Bluetooth running Ubuntu Linux
- 1) MicaSense RedEdge calibration panel

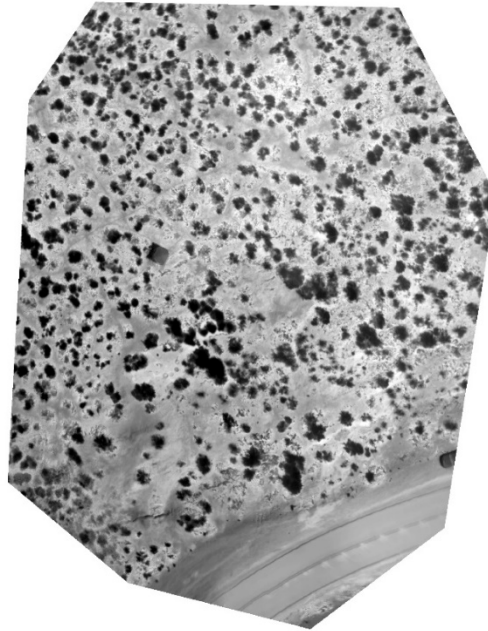
# Appendix B Imagery and Probability Oil Maps

## McKittrick – Flight 1

McKittrick - Multispectral RGB Composite

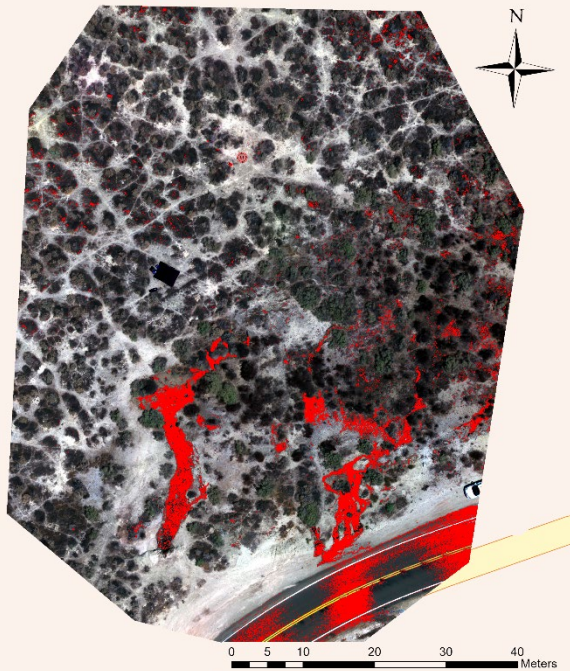


McKittrick TIR



UAS Flight 1 - Probable Oil Map | McKittrick Tar Pits

Date: June 8th, 2021  
Time: 11:36 - 11:41am PST  
Altitude: 40 m

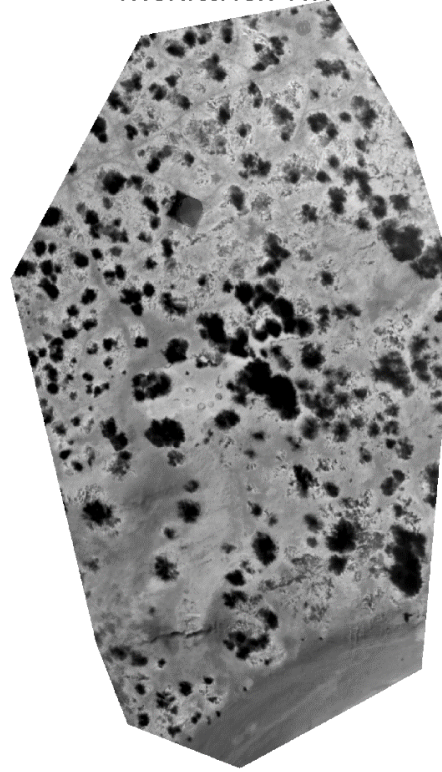


## McKittrick – Flight 2

McKittrick - Multispectral RGB Composite

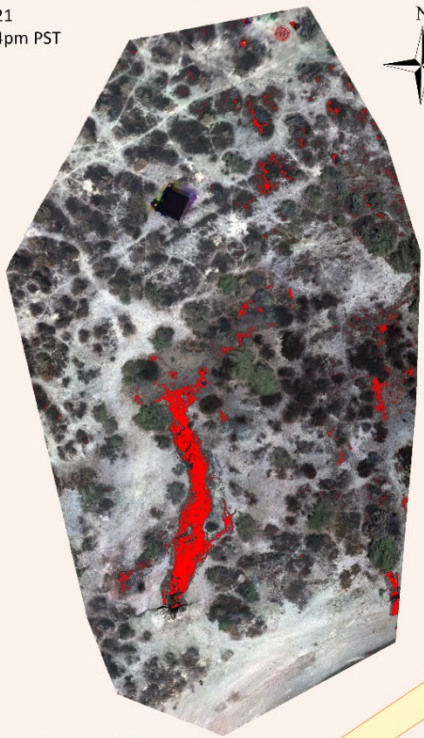


McKittrick TIR



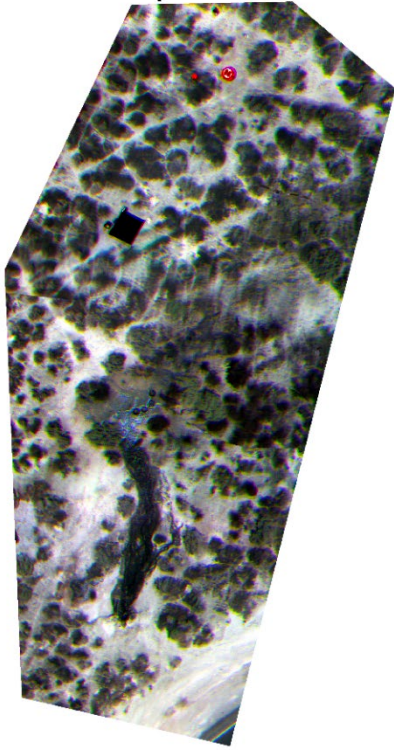
UAS Flight 2 - Probable Oil Map | McKittrick Oil Fields

Date: June 8th, 2021  
Time: 12:21 - 12:24pm PST  
Altitude: 20 m

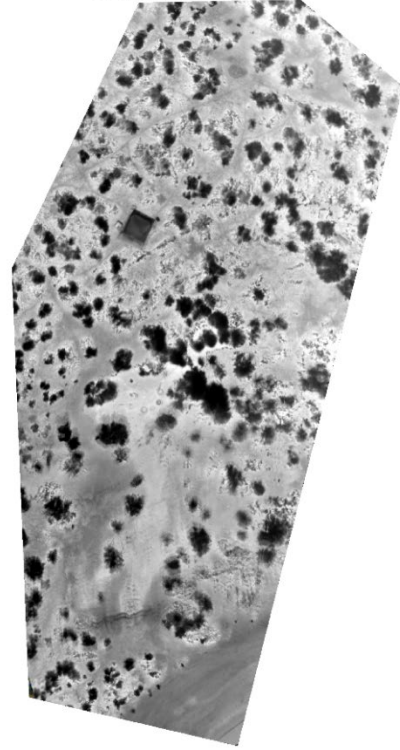


### McKittrick – Flight 3

McKittrick - Multispectral RGB Composite

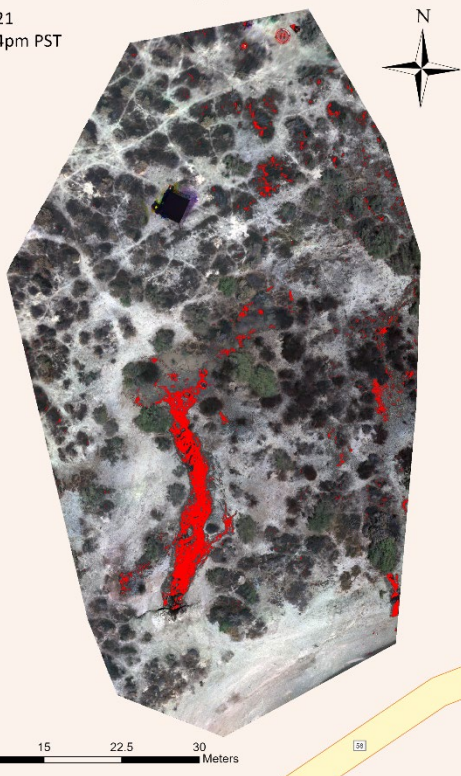


McKittrick TIR



### UAS Flight 2 - Probable Oil Map | McKittrick Tar Pits

Date: June 8th, 2021  
Time: 12:21 - 12:24pm PST  
Altitude: 20 m

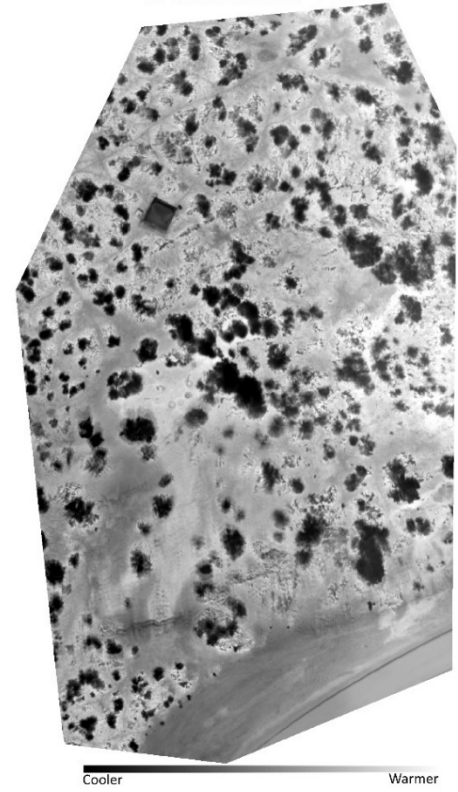


# McKittrick – Flight 4

McKittrick - Multispectral RGB Composite

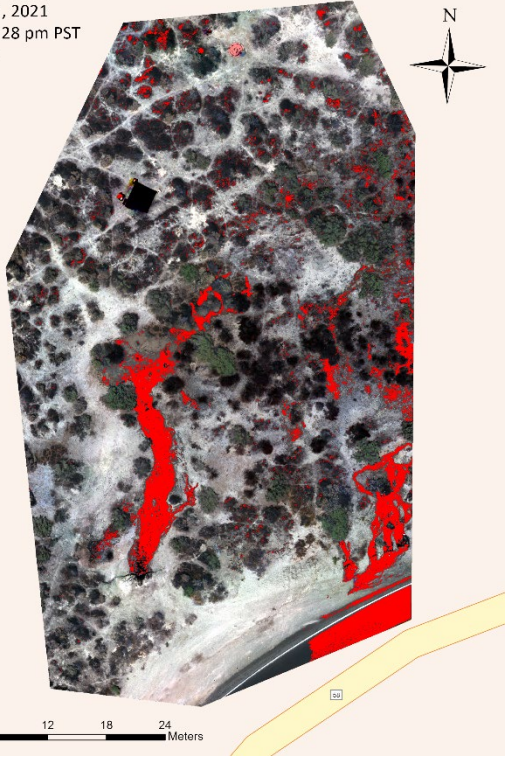


McKittrick TIR



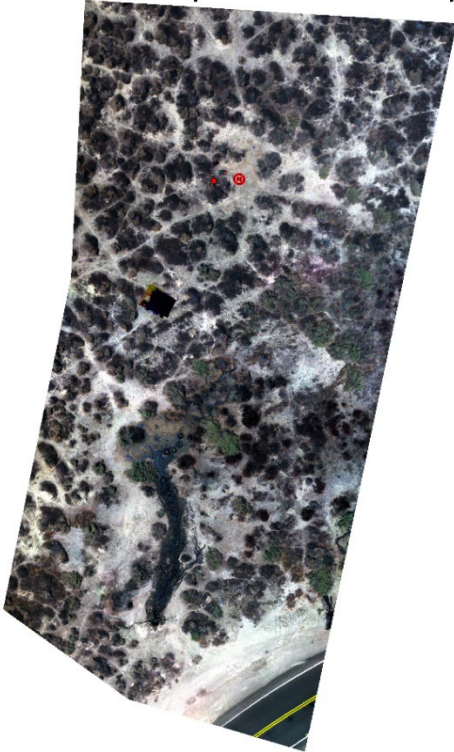
UAS Flight 4 - Probable Oil Map | McKittrick Tar Pits

Date: June 8th, 2021  
Time: 1:24 - 1:28 pm PST  
Altitude: 30 m

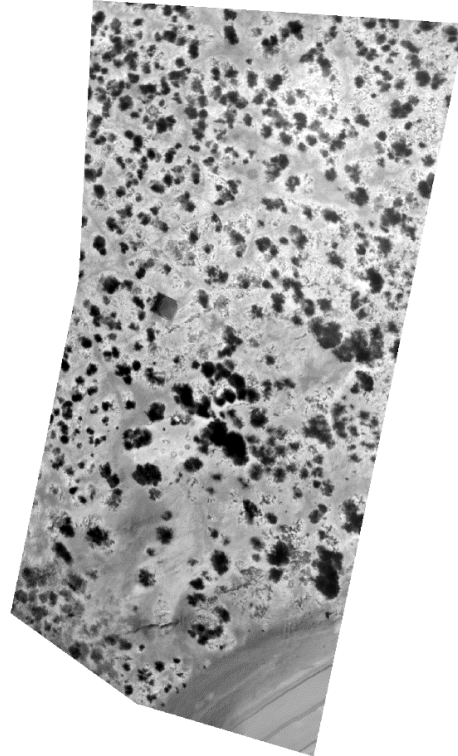


# McKittrick – Flight 5

McKittrick - Multispectral RGB Composite

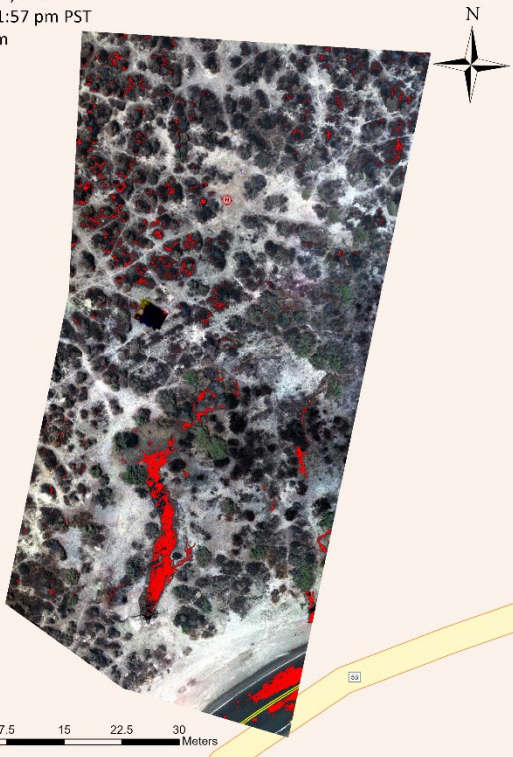


McKittrick TIR



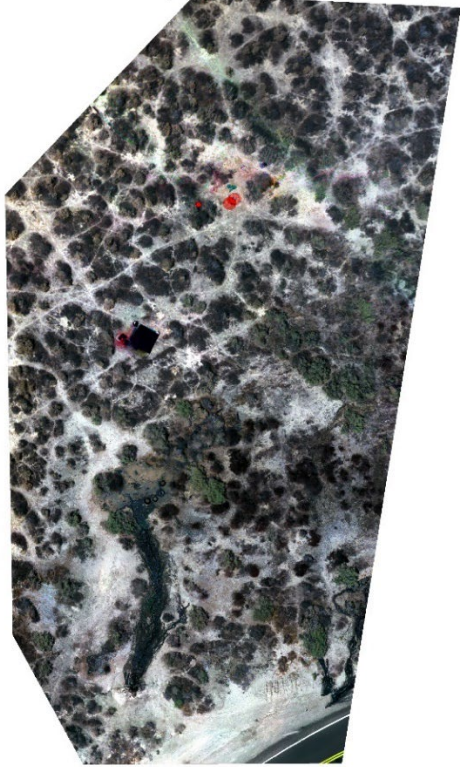
## UAS Flight 5 - Probable Oil Map | McKittrick Tar Pits

Date: June 8th, 2021  
Time: 1:54 - 1:57 pm PST  
Altitude: 20 m

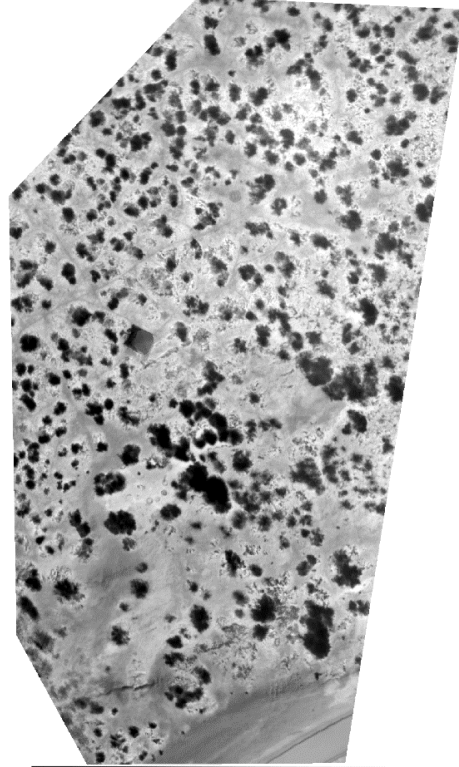


# McKittrick – Flight 6

McKittrick - Multispectral RGB Composite

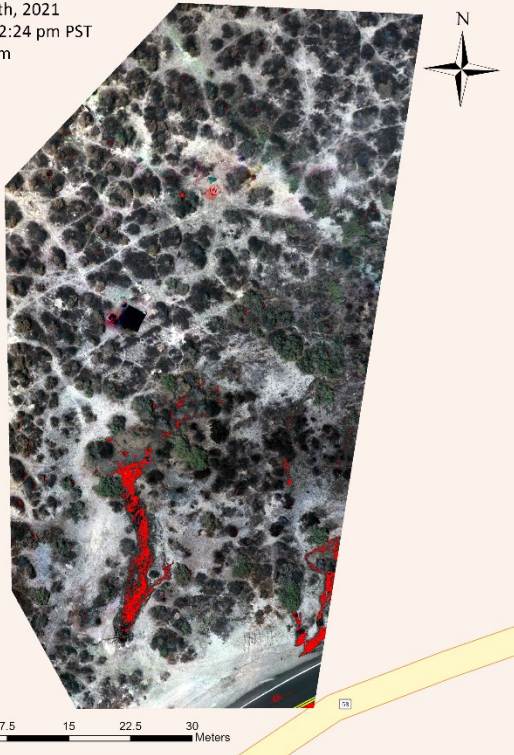


McKittrick TIR



UAS Flight 6 - Probable Oil Map | McKittrick Tar Pits

Date: June 8th, 2021  
Time: 2:20 - 2:24 pm PST  
Altitude: 20 m

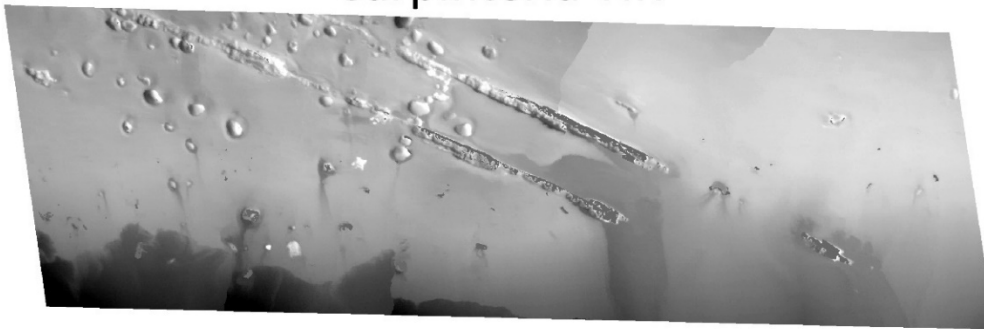


## Carpinteria – Flight 1

### Carpinteria - Multispectral RGB Composite



### Carpinteria TIR



Cooler  Warmer

### UAS Flight 1 - Probable Oil Map | Carpinteria Bluffs

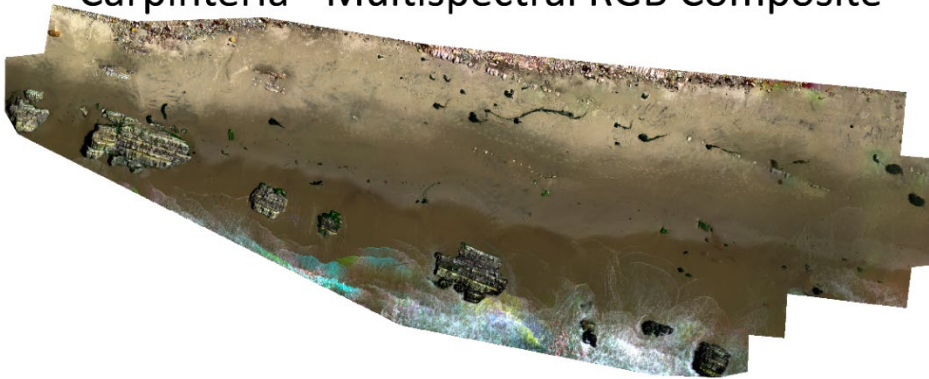
Date: June 10th, 2021  
Time: 9:38 - 9:48 am PST  
Altitude: 20 m



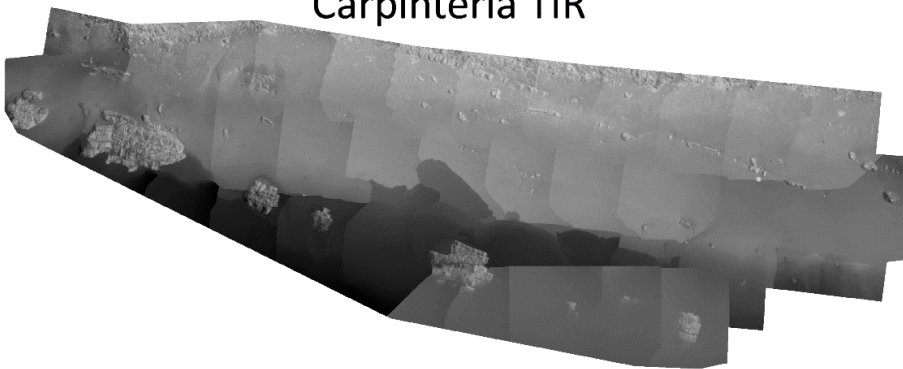
0 2.5 5 10 15 20 Meters

## Carpinteria – Flight 2

### Carpinteria - Multispectral RGB Composite



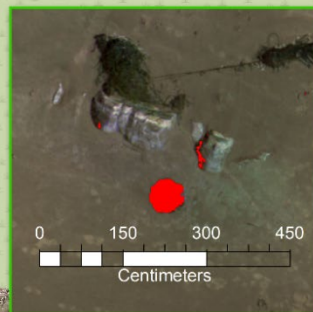
### Carpinteria TIR



Cooler Warmer

### UAS Flight 2 - Probable Oil Map | Carpinteria Bluffs

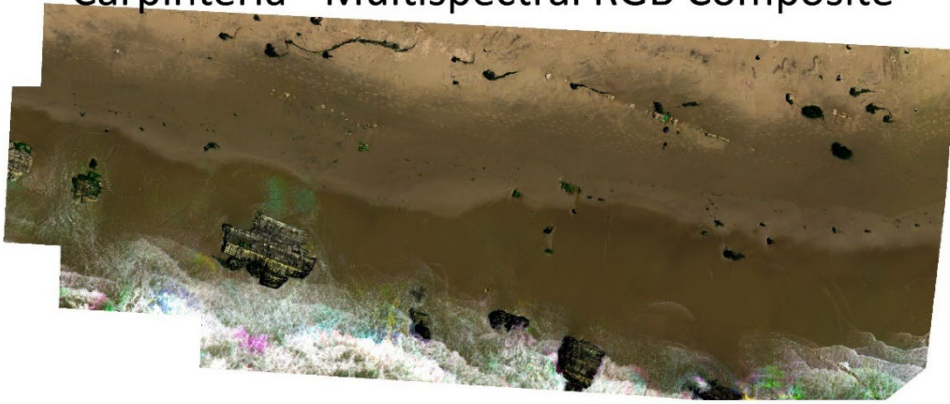
Date: June 10th, 2021  
Time: 10:20 - 10:27am PST  
Altitude: 20 m



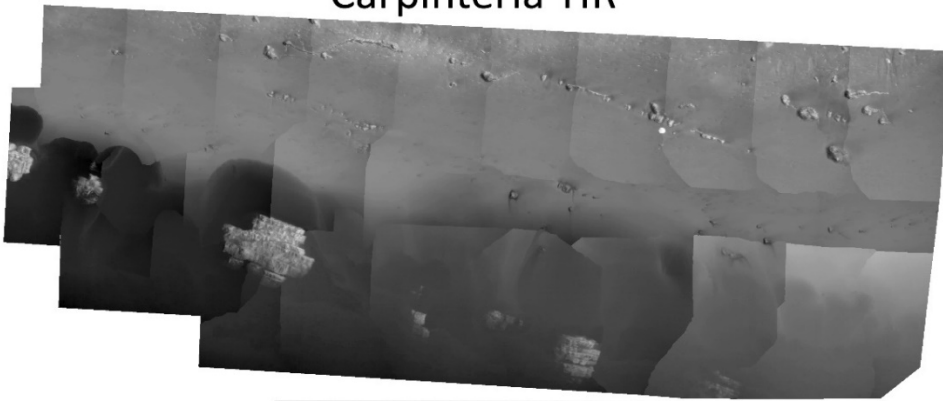
0 5 10 20 30 40 Meters

## Carpinteria – Flight 3

### Carpinteria - Multispectral RGB Composite



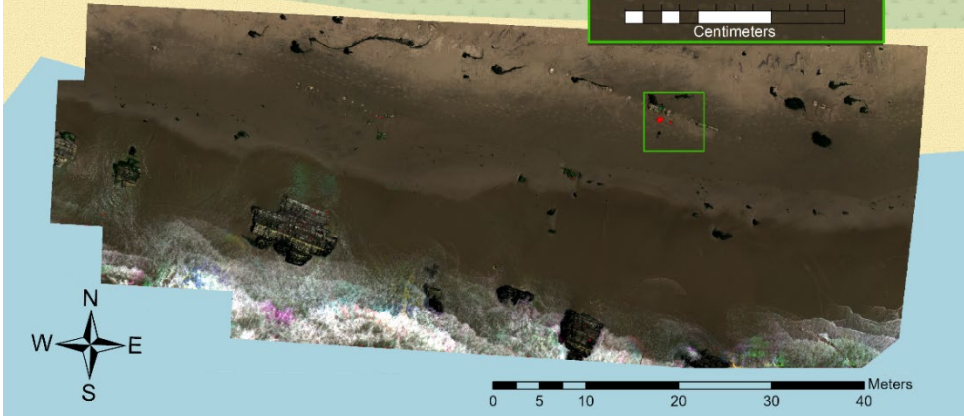
### Carpinteria TIR



Cooler Warmer

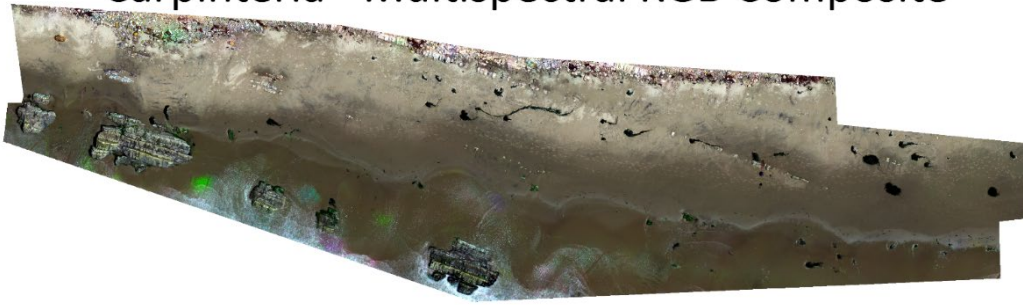
### UAS Flight 3 - Probable Oil Map | Carpinteria Bluffs

Date: June 10th, 2021  
Time: 10:54 - 11:00am PST  
Altitude: 10 m

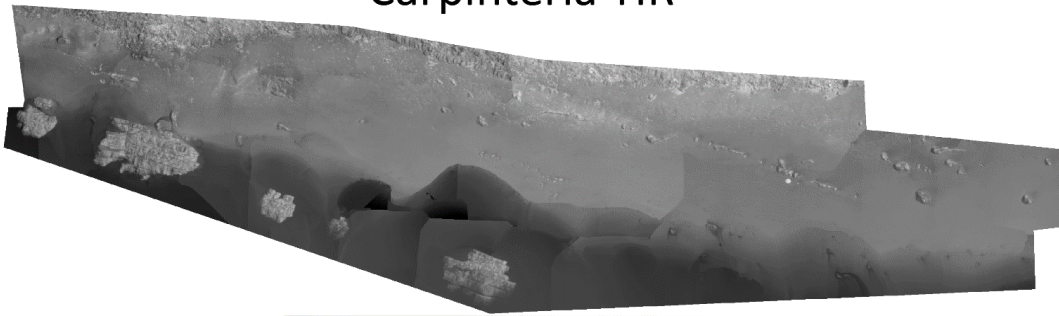


# Carpinteria – Flight 4

## Carpinteria - Multispectral RGB Composite



## Carpinteria TIR



Cooler  Warmer

## UAS Flight 4 - Probable Oil Map | Carpinteria Bluffs

Date: June 10th, 2021  
Time: 11:17 - 11:24am PST  
Altitude: 30 m

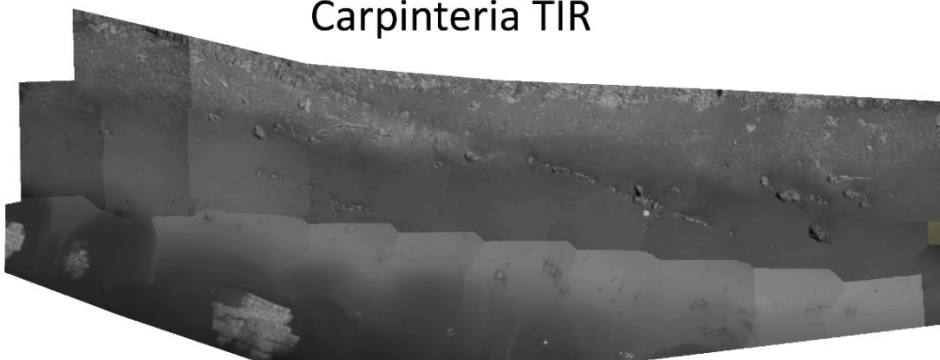


## Carpinteria – Flight 5

### Carpinteria - Multispectral RGB Composite



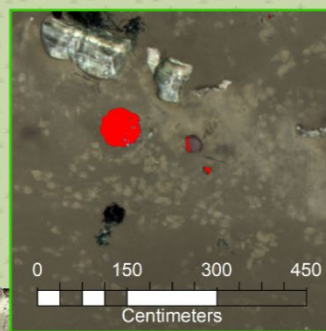
### Carpinteria TIR



Cooler Warmer

### UAS Flight 5 - Probable Oil Map | Carpinteria Bluffs

Date: June 10th, 2021  
Time: 12:02 - 12:06pm PST  
Altitude: 20 m



0 5 10 20 30 40 Meters